Received: 29 July 2025 | Revised: 9 January 2026 | Accepted: 15 January 2026

DOI: 10.1002/ar.70156

RESEARCH ARTICLE

The Anatomical Record | American Association for Anatomy | WILEY

Integrating whole-bone and regional analyses to understand human scapular growth

Azahara Salazar-Fernández[1] | **José Miguel Carretero**[1,2] | **Laura Rodríguez**[1,3] | **Rebeca García-González**[1]

[1]Laboratorio de Evolución Humana, Universidad de Burgos, Edificio I+D+i/CIBA, Burgos, Spain

[2]Unidad Asociada de I+D+i al CSIC Vidrio y Materiales del Patrimonio Cultural (VIMPAC), Burgos, Spain

[3]Departamento de Biodiversidad y Gestión Ambiental, Facultad de Ciencias Biológicas y Ambientales, Universidad de León, León, Spain

Correspondence
Rebeca García-González, Laboratorio de Evolución Humana, Universidad de Burgos, Edificio I+D+i/CIBA, Plaza Misael Bañuelos s/n, 09001 Burgos, Spain.
Email: mrgarcia@ubu.es

Funding information
Junta de Castilla y León and Fondo Europeo de Desarrollo Regional; Ministerio de Ciencia, Innovación y Universidades, Grant/Award Number: PID2021-122355NB-C31

Abstract

This study investigates ontogenetic changes in human scapular morphology using three-dimensional geometric morphometrics with whole-bone and region-specific analyses. The aim is to evaluate whether the scapula follows a regular developmental pattern and whether its functionally distinct components, the scapular spine (SS) and glenoid fossa (SGF), exhibit divergent growth trajectories indicative of modular development. This approach assesses interactions between global and local morphological change and explores the influence of size, biomechanics, and ossification timing on scapular development. We analyzed 3D surface scans of 127 scapulae from non-adult and adult individuals from the medieval San Pablo Collection, Spain, and the documented Lisbon Collection, Portugal. Seven ontogenetic groups were defined using dental and chronological age. Landmark and semi landmark configurations were generated for the entire scapula, the scapular spine, and the glenoid fossa. Shape and form variation were examined using Generalized Procrustes Analysis and Principal Component Analysis. Across all regions, PC1 captured the main axis of ontogenetic variation, separating age groups in both shape and form space. Whole-scapula analyses revealed a gradual developmental pattern, whereas regional analyses highlighted distinct trajectories. The scapular spine showed progressive curvature and torsion, likely reflecting muscular loading, while the glenoid fossa displayed more constrained changes linked to joint stabilization and ossification timing. These findings support a modular model of scapular growth, with regions responding to intrinsic developmental processes and extrinsic biomechanical influences. Integrating regional and whole-bone analyses reveals developmental plasticity not detectable through global approaches alone, with implications for forensic, clinical, paleoanthropological, and bioarchaeological research.

KEYWORDS

glenoid cavity, modularity, musculoskeletal growth, ontogeny, scapular spine

1 | INTRODUCTION

The study of skeletal development in non-adult individuals has gained considerable attention in recent decades, driven by a growing interest in understanding growth patterns and adaptations in both past and present populations. Bioarcheological research has predominantly focused on the growth patterns of the long limb bones, with numerous studies comparing these patterns across temporally, geographically, and ecologically diverse groups (see Humphrey, 2000, for a review). Additionally, much effort has been dedicated to refining age estimation methods (Cardoso et al., 2014; Cowgill et al., 2010; López-Costas et al., 2012; Rissech et al., 2008, 2013; Stull et al., 2014).

In contrast, the growth of other bones associated with other dimensions of the skeleton, such as the scapula and clavicle, has received relatively less attention, both in modern humans (Black & Scheuer, 1996; Bleuze et al., 2016; Cardoso et al., 2017; Frelat et al., 2017; Humphrey, 1998; McGraw et al., 2009; Rissech & Black, 2007) and in fossil hominins (García-González et al., 2009; García-González, Rodríguez, Salazar-Fernández, et al., 2024; Rosas et al., 2017). Although these studies highlight the importance of shoulder girdle development for advancing our understanding of overall skeletal growth and their potential applications in evolutionary research on age estimation, most have focused primarily on the increase in the size of the clavicle and scapula.

Nevertheless, skeletal development involves not only increases in size but also changes in shape (Roche, 1992). Understanding how shape varies throughout ontogeny has become a central focus in studies of morphological development and functional adaptation. In this context, several studies have shown that scapular shape differences throughout development among different hominin species can be associated with changes in locomotor behavior or activity-related adaptations (Churchill & Rhodes, 2009; Churchill & Trinkaus, 1990; Green & Alemseged, 2012; Trinkaus, 1977). However, Di Vincenzo et al. (2012) argued that the differences observed between *Homo sapiens* and most fossil hominins reflect an evolutionary developmental trend rather than adaptive morphological responses to mechanical stress at the shoulder joint.

These seemingly contradictory results may arise from differences in methodologies for size and shape estimation (e.g., linear and angular measurements vs. three-dimensional geometric morphometrics [3DGM]), or from varying research foci, such as examining the entire scapula versus only a region of it (e.g., the scapular glenoid fossa [SGF]). Despite recent progress, the relationship between global and region-specific patterns of scapular growth, as well as their implications for modularity and developmental plasticity, remains poorly understood and underscores the importance of investigating both ontogenetic trajectories and intraindividual variability when analyzing scapular development. Considering the scapula's morphological complexity (Ogden & Phillips, 1983; Scheuer & Black, 2000) (Figure 1), a comprehensive approach that captures both size and shape variation, as well as regional differentiation, is essential.

A useful comparative framework comes from hominoids. For example, some studies using 3DGM in anthropoid primates have provided valuable insight into this debate (Young, 2006, 2008). These studies point toward a combination of embryonic and epigenetic influences, rather than postnatal mechanical loading alone, as primary drivers of shape variation. Additionally, Young (2004) evaluated the modularity of the hominoid scapula and showed that its anatomy can be partitioned into functionally meaningful modules, which typically include the scapular blade, the scapular spine (SS) with its distal extension (the acromion), the SGF, and the coracoid process. The study also demonstrated that the degree of integration among these regions varies across taxa. This modular perspective helps explain how different anatomical areas accommodate distinct functional demands, such as glenohumeral stability, load transmission, and extensive muscular attachment.

In contrast, explicit tests of scapular modularity in humans are scarce, particularly during ontogeny. Building on Young's comparative insights, we posit that analogous modular differentiation may operate in the human scapula, and that growth trajectories of these regions could diverge due to a combination of genetic and biomechanical influences. Accordingly, we combine a global analysis of the entire bone with focused assessments of two anatomically and functionally distinct regions: the SGF (including the superior coracoid) and the SS. We employ 3DGM to quantify both size and shape variation across ontogeny with higher precision. This design allows us to (i) test whether the scale of anatomical analysis affects the detection of developmental differences, (ii) evaluate patterns of integration and modularity during growth, and (iii) gauge the potential for developmental plasticity. We predict that region-specific analyses will reveal developmental patterns that may remain obscured in whole-bone analyses, allowing a more precise assessment of shape changes and integration during growth. In particular, we expect differences between the ontogenetic trajectories of the SGF and the SS, reflecting their distinct developmental timing and functional roles. By comparing these regional trajectories, we can also assess the relative influence of developmental timing and biomechanical factors on scapular shape change, providing new insights into how both

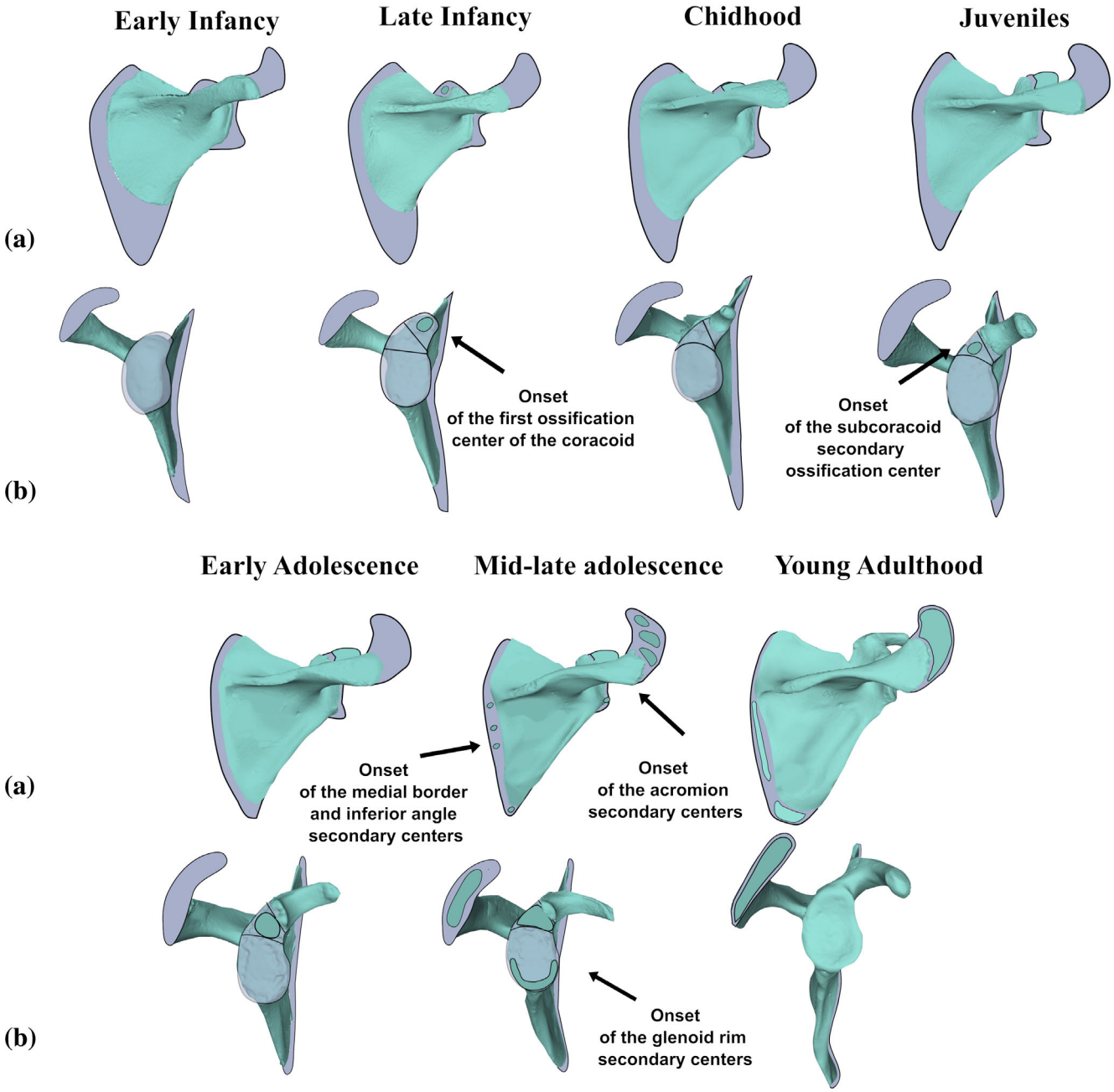

FIGURE 1 Ontogenetic sequence of non-adult scapulae in posterior (a) and medial (b) views. The three-dimensional models are based on radiographic images provided by Ogden and Phillips (1983). The cartilaginous mass (shown in gray) serves as a developmental template for future bone formation and is most prominent in the regions of the acromion, the glenoid–coracoid interface, and the medial border. The coracoid ossification center is always present within the first year of life. During late infancy, it increases in size, and by around 3 years of age it acquires its characteristic hook-like morphology. It fuses with the rest of the scapula by mid-adolescence. Juvenile individuals begin ossifying the first secondary center of the scapula—the subcoracoid. The remaining secondary ossification centers do not appear until mid-adolescence.

processes contribute to the emergence of modularity and integration during ontogeny. This region-specific perspective also enhances the applicability of our approach to fragmentary archeological material and provides a comparative bridge to future work spanning humans and non-human primates.

2 | MATERIALS AND METHODS

2.1 | Sample

The total sample used in this study comes from two different osteological collections: the San Pablo medieval

collection, housed at Laboratory of Human Evolution of the University of Burgos and the contemporary Lisbon collection, housed at Natural History Museum (Lisbon, Portugal) (Table 1).

The San Pablo sample dates to between the 14th and 18th centuries, with age at death in non-adult individuals estimated from (i) dental mineralization stages via Computed Tomography (CT) scans following Demirjian et al. (1973), and (ii) using age standards from Liversidge et al. (2006) for permanent dentition and Liversidge and Molleson (2004) for deciduous dentition. These samples have been previously studied in terms of growth and development (García-González, 2013; García-González, Rodríguez, Salazar-Fernández, et al., 2024), showing that some individuals experienced delayed skeletal development, likely due to malnutrition and illness. However, this delay did not impact humeral development (Salazar-Fernández, Carretero, Quintino, et al., 2025) or the modeling process, as assessed through the cross-sectional properties of the femur (Muñoz-Guarinos et al., 2025) and the occipital bone (Lozano-Bendicho et al., 2025).

The second sample derives from the Luís Lopes Collection (Lisbon Collection), curated at the Bocage Museum (National Museum of Natural History, Lisbon, Portugal), and consists of individuals of known sex and age at death from 19th- and 20th-century municipal cemeteries in Lisbon. The collection has been assembled since 1981 with authorization from the Lisbon City Council to recover skeletal remains legally unclaimed after exhumation from temporary graves (Cardoso, 2006). In Lisbon cemeteries, individuals are exhumed after the legally mandated 5-year burial period to allow grave reuse; unclaimed remains destined for communal burial or destruction are recovered by the Museum for scientific study. Many individuals in this collection exhibit delayed skeletal growth and maturation due to socioeconomic factors (Cardoso, 2007; Conceição & Cardoso, 2011). The main difference between these two skeletal collections is the use of different age estimation methods: actual chronological age for the Lisbon collection and estimated age for the San Pablo collection as mentioned above. The Liversidge et al. (2006) method has a mean error of only −0.21 years (Liversidge et al., 2010), meaning these discrepancies are unlikely to significantly affect our analysis of scapular developmental changes. Additionally, the broad maturity stages analyzed in this study (see below) help minimize potential biases from minor differences in age estimation. Moreover, previous studies have shown that there are no differences in the growth and developmental pattern between these two skeletal collections (García-González et al., 2019; Salazar-Fernández, Carretero, Quintino, et al., 2025). Therefore, they were grouped together to maximize the sample size (Table 1).

TABLE 1 Sample used in this study.

	San Pablo	Lisbon	Total
Complete scapula	28	39	67
Scapular spine	68	43	111
Scapular glenoid fossa	46	38	84

The sample was divided into seven maturity groups for the entire scapular morphology (ESM) and SS analyses, ranging from birth to adulthood, based on the ontogenetic pattern of the scapula (Figure 1) and general stages of human growth and development (Bogin, 2021; Cardoso et al., 2017; García-González, Rodríguez, Salazar-Fernández, et al., 2024; Kothary et al., 2014; Ogden & Phillips, 1983; Rissech & Black, 2007; Salazar-Fernández, Carretero, Rodríguez, & García-González, 2025; Scheuer & Black, 2004) (Table 2). For individuals older than 18 years, only those in which the acromion body remained unfused, or in which a visible fusion line allowed clear identification of the independent acromial epiphysis, were considered. To further investigate this region, a separate analysis was conducted including fragmented scapulae with a well-preserved SS, focusing specifically on changes in curvature and assuming the same maturity groups as for the ESM analysis. This preservation condition explains why the number of ESM was 67 specimens, which is smaller than the sample available for region-specific analyses of the SS (111 specimens).

The range of maturity groups established for the ESM and SS analyses is not compatible with a morphological study of the SGF, due to characteristic development. At birth, the glenoid surface is almost oval in shape and extends onto the superior and ventral aspects to articulate with the coracoid process. Growth in the glenoid–coracoid region is driven by the development of a bipolar growth plate, which appears around the second year of life and enables endochondral ossification to proceed in two opposite directions (Ogden & Phillips, 1983). Unlike a conventional growth plate, where endochondral ossification proceeds in a single direction, the bipolar growth plate exhibits ossification progressing in two opposite directions, diverging from a central reserve zone (Kothary et al., 2014). This bipolar growth plate promotes bony expansion both toward the coracoid process and across the non-ossified glenoid surface. Two secondary centers of ossification are associated with this area: the subcoracoid center, located in the superior third of the glenoid surface and dorsal to the base of the coracoid process, and a glenoid epiphyseal center corresponding to the remainder of the glenoid surface (Kothary et al., 2014). The subcoracoid center usually appears around 8 years of age, while the glenoid epiphyseal center develops shortly thereafter. Both centers typically

fuse with each other and with the coracoid process between 15 and 17 years of age, either sequentially or simultaneously, forming a single continuous epiphysis that completes the glenoid cavity (Scheuer & Black, 2000, 2004). Given this developmental sequence, the maturity groups used for the SGF analysis were adjusted accordingly. The first maturity group defined for the ESM and SS regions was not included in the SGF analysis, since bipolar growth cannot yet be assessed at this early stage. The third maturity group was extended to include individuals up to 8 years of age, and the fourth group was defined from 8 to 10 years, with 8 years marking the onset of the subcoracoid ossification center. The sixth maturity group was limited to 16 years, corresponding to the period when the subcoracoid and coracoid centers begin to fuse, making the landmark configuration no longer comparable across specimens. Consequently, the seventh maturity group was excluded from the SGF analysis. In total, SGF from 84 individuals was analyzed (Table 2).

2.2 | Data acquisition

Both collections were digitized using three-dimensional (3D) surface scanners to generate high-resolution models: a 3D laser scanner (NextEngine Desktop 3D) and a structured-light scanner (EinScan Pro). Although laser scanners may operate more slowly, both methods have been validated as reliable tools for anthropological research (Almécija et al., 2024). The Lisbon sample was digitized using the NextEngine software, ScanStudio HD (version 1.3.2). Each scapula was scanned from three different views using a 360° positioning system with an automatic turntable, acquiring 30 individual scans per view with a maximum accuracy of 0.1 mm. Each view was subsequently post-processed to clean the scans and then combined into a single high-resolution 3D model through manual placement of homologous points. Depending on the size of the bone, either Macro Mode (±0.13 mm accuracy) or Wide Mode (±0.38 mm

TABLE 2 Maturity groups based on scapular developmental changes.

Maturity group	Age range	*N* (ESM)	*N* (SS)	*N* (SGF)	Key developmental events
First maturity group. Early infancy[a]	0–1	8	12	-	First appearance of the coracoid process. The subchondral osseous contour of the glenoid is either flat or slightly convex and minimally retroverted.
Second maturity group. Late infancy	1–3	9	15	22	Establishment of the bipolar growth plate.
Third maturity group. Childhood	3–6	8	15	17	Progressive replacement of the vertebral border cartilage by the advancing endochondral ossification, except inferiorly.
Fourth maturity group. Juvenility[b]	6–10	9	13	15	First appearance, formation and expansion of the subcoracoid process.
Fifth maturity group. Early adolescence	10–14	10	18	18	Subcoracoid and coracoid process begin approaching each other. The subchondral osseous contour of the glenoid assumed a concave contour comparable to the articular surface.
Sixth maturity group. Mid-late adolescence[c]	14–18	15	21	12	Fusion between coracoid, subcoracoid and body of scapula, as well as of the glenoid rim epiphysis. First appearance of acromial epiphysis and epiphysis for inferior angles.
Seventh maturity group. Adulthood[d]	≥18	8	17	-	Fusion of the acromion, the inferior angle and the medial border.

Abbreviations: ESM, entire scapular morphology; SGF, scapular glenoid fossa; SS, scapular spine.

[a]This group was not included in the analysis of scapular glenoid fossa development due to the bipolar growth plate having not yet formed in the sample.

[b]This group is subdivided for the analysis of scapular glenoid fossa development: up to 8 years (before the appearance of the subcoracoid process) and 8–10 years (during its expansion).

[c]In the analysis of the scapular glenoid fossa, this group includes individuals up to 16 years of age, when the subcoracoid and coracoid epiphyses are fused.

[d]This group was not included in the analysis of the scapular glenoid fossa development.

accuracy) was used. The San Pablo sample was scanned with the structured-light scanner in fixed mode using an automatic turntable, achieving a scanning accuracy of 0.04 mm per scan. Each scapula was scanned from three views, each composed of 30 individual scans spanning 360° arcs. All scans were then aligned and automatically merged into a single 3D model using the ExScan Pro software (ExScan Pro, Solid Edge SHINING 3D Edition). For both collections, the scapula was scanned in the same three views: in the first view, the scapula was positioned vertically with the inferior angle resting on the turntable; in the second view, it was placed horizontally with the lateral edge of the spine on the turntable; and in the third view, the medial portion of the spine rested on the turntable. When the height of the bone relative to the scanner required adjustment, the Lisbon turntable was slightly elevated using a stable support, whereas the San Pablo scanner could be positioned at different heights using a tripod. Subsequently, all scans underwent alignment and merging processes to form a unified 3D model. All final models requiring minor refinements were exported as .ply files to Autodesk Meshmixer (RRID:SCR_015736) for adjustments, such as closing small holes.

2.3 | Three-dimensional geometric morphometric analysis

Three different sets of 3D landmark configurations were created, one for each analysis (Figure 2, Table 3). The first analysis involves the ESM configuration with nine fixed landmarks located at different relevant anatomical points of the scapula which are equivalent to the terminal points of linear variables (Cardoso et al., 2017; Rissech & Black, 2007). The second analysis, focusing on the SS, is composed of six fixed landmarks and 38 curve semi-landmarks and is designed to outline the borders of the superior and inferior curvatures of the SS in order to quantify in detail its developmental trajectories (Figure 2, Table 3). The third analysis focuses on the SGF and consists of 8 fixed landmarks and 36 curve semi-landmarks, which delineate the contour of the subadult glenoid cavity (Figure 2, Table 3).

Semi-landmarks were slid along their corresponding curves with respect to the fixed landmarks in order to minimize bending energy. This procedure was performed first between each specimen and the template (using an initial random specimen) and then again against the average sample configuration (Bastir et al., 2013; Mitteroecker & Gunz, 2009). All landmark configurations were created in Checkpoint software (Stratovan Corporation, Davis, CA, USA, 2018) where digitation was made by the same researcher (AS-F) to avoid interobserver measurement error. This same software was then utilized to apply each template configuration to its respective sample in order to minimize bending energy between the sample and the template (Gunz et al., 2006; Gunz & Mitteroecker, 2013; Slice, 2005). The raw coordinates of the landmarks and semi-landmarks were then imported into MorphoJ (Klingenberg, 2011) for a Generalized Procrustes Analysis (GPA) (Rohlf & Slice, 1990; Slice, 2005). This Procrustes superimposition method minimizes discrepancies between corresponding landmarks, with size being represented by a scaling factor called centroid size. This process enables the conversion of raw coordinates into Procrustes shape coordinates (Bookstein, 2018; Rohlf & Slice, 1990). The Procrustes coordinates were then exported to the PAST 4.13 software package (Hammer-Muntz et al., 2001), where a principal component analysis (PCA) was conducted on the entire sample set for each scapular analysis. The broken stick method (Frontier, 1976) was used to identify the principal components that account for a statistically significant proportion of variance. This method provides an objective criterion for selecting meaningful axes of variation by comparing the observed eigenvalues with those expected under a random (null) distribution, retaining only components that explain more variance than would be expected by chance. In addition to the shape analysis, a form analysis (defined as shape plus size) was performed by adding the natural logarithm of centroid size (lnCS) as an additional variable to the Procrustes shape coordinates (Mitteroecker et al., 2004). The inclusion of lnCS ensures that the distribution in size-and-shape space is isotropic for landmark variation. This variable was incorporated into the PCA, where the distance in this space can be interpreted as a measure of form differences. Considering both form and shape, provides complementary perspectives on scapular development (e.g., Freidline et al., 2013; Mori & Harvati, 2019). While the shape space isolates variation independent of size, the form space retains both size and shape information, allowing us to evaluate how allometric effects contribute to ontogenetic trajectories.

3 | RESULTS

According to the broken stick criteria (Frontier, 1976), the relative warps analysis of ESM produced only three statistically significant PCs that explain 67.1% of the total variance (Figure 3a). PC1 and PC2 together explained 57.3% of the total variance and 85.4% of the significant variance. For the SS, six PCs were identified as statistically significant, explaining 82.5% of the total variance (Figure 3b). In this case, PC1 and PC2 together accounted for 55.7% of the total variance and 67.6% of the significant

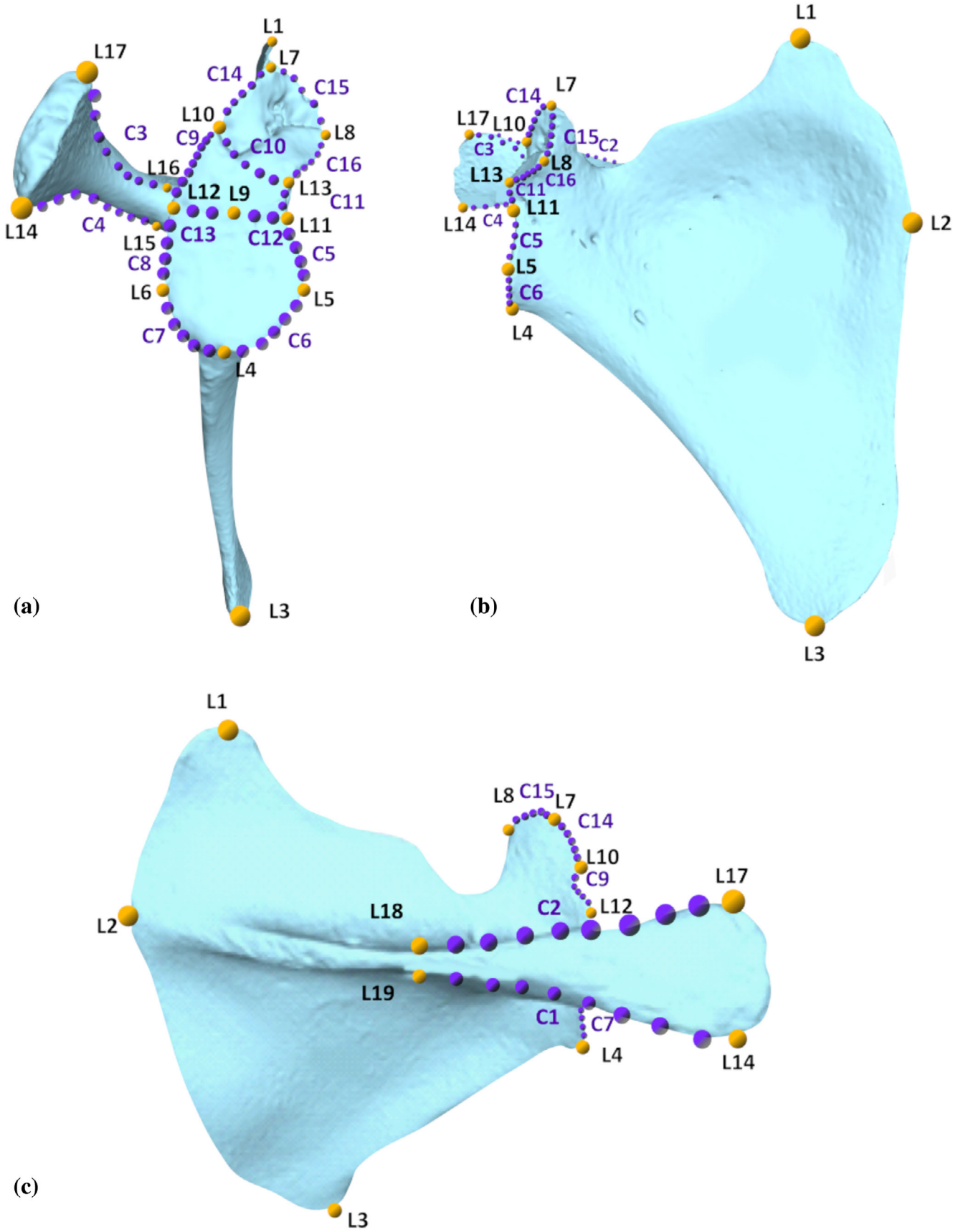

FIGURE 2 Global view regarding the three set of landmarks (yellow dots) and curved semi-landmarks (blue dots) used for the analyses. (a) Lateral view. (b) Anterior view. (c) Superoposterior view.

TABLE 3 Set of landmarks and semi-landmarks.

Number	Description of the point
L_1	The most superior point of the superior angle.
L_2	The most medial point of the scapular spine at the vertebral border.
L_3	The most inferior point of the inferior angle.
L_4	The most inferior point of the glenoid fossa.
L_5	The most anterior point of the glenoid fossa in relation to the anatomical orientation of the scapula.
L_6	The point located most posteriorly within the glenoid fossa relative to the anatomical orientation of the scapula.
L_7	The most posteromedial point of the coracoid metaphyseal surface.
L_8	The most anteromedial point of the coracoid metaphyseal surface.
L_9	The central superior point of the inferior two-thirds of the glenoid fossa.
L_10	The most superior point of the subcoracoid metaphysis.
L_11	The most anterosuperior point of the inferior two-thirds of the glenoid cavity.
L_12	The most posterosuperior point of the inferior two-thirds of the glenoid cavity.
L_13	At the scapular notch, the junction between the subcoracoid and coracoid methaphyses of the scapula.
L_14	The most inferolateral point of the scapular spine.
L_15	The most inferior point at the deepest area of the spinoglenoid notch.
L_16	The most superior point at the deepest area of the spinoglenoid notch.
L_17	The most superolateral point of the scapular spine.
L_18	The most superior point of the midpoint of the scapular spine.
L_19	The most inferior point of the midpoint of the scapular spine.
Curve_1	Along the inferior border of the scapular spine among the fixed landmarks 19 and 14. Total: 8 semi-landmarks.
Curve_2	Along the superior border of the scapular spine among the fixed landmarks 18 and 17. Total: 8 semi-landmarks.
Curve_3	Along the superior border of the inner scapular spine and spinoglenoid notch among the fixed landmarks 17 and 16. Total: 8 semi-landmarks.
Curve_4	Along the inferior border of the inner scapular spine and spinoglenoid notch among the fixed landmarks 14 and 15. Total: 8 semi-landmarks.
Curve_5	Along the superoanterior border of the two inferior thirds of the glenoid cavity, among the fixed landmarks 11 and 5. Total: 4 semi-landmarks.
Curve_6	Along the inferoanterior border of the two inferior thirds of the glenoid cavity, among the fixed landmarks 5 and 4. Total: 5 semi-landmarks.
Curve_7	Along the inferoposterior border of the two inferior thirds of the glenoid cavity, among the fixed landmarks 4 and 6. Total: 5 semi-landmarks.
Curve_8	Along the superoposterior border of the two inferior thirds of the glenoid cavity, among the fixed landmarks 6 and 12. Total: 4 semi-landmarks.
Curve_9	Along the posterior border of the subcoracoid, among the fixed landmarks 12 and 10. Total: 8 semi-landmarks.
Curve_10	Along the boundary between the coracoid and subcoracoid scapular metaphyses among the fixed landmarks 10 and 13. Total: 5 semi-landmarks.
Curve_11	Along the scapular notch in the subcoracoid scapular metaphysis among the fixed landmarks 13 and 11. Total: 2 semi-landmarks.
Curve_12	Along the border separating the superior area of the inferior two-thirds of the glenoid cavity and the surface of the subcoracoid metaphysis among the fixed landmarks 9 and 11. Total: 2 semi-landmarks.
Curve_13	Along the border separating the superior area of the inferior two-thirds of the glenoid cavity and the surface of the subcoracoid metaphysis among the fixed landmarks 9 and 12. Total: 2 semi-landmarks.
Curve_14	Along the posterior border of the coracoid metaphyseal surface, among the fixed landmarks 10 and 7. Total: 5 semi-landmarks.
Curve_15	Along the medial border of the coracoid metaphyseal surface, among the fixed landmarks 7 and 8. Total: 5 semi-landmarks.
Curve_16	Along the anterior border of the coracoid metaphyseal surface, among the fixed landmarks 8 and 13. Total: 5 semi-landmarks.

variance. Finally, in the SGF analysis, only eight PCs were considered significant, explaining 76% of the total shape variability (Figure 3c), with PC1 and PC2 together accounting for 43.8% of total variance and 57.5% of significant variance. In all three analyses, PC1 accounted for a higher proportion of variance in form space than in shape space because, in the former, PCs also captured variation in size. The higher percentage of explained variance (94.8% for the ESM, 88.3% for the SS, and 93.9% for the SGF), reflects the strong influence of allometric growth and size-related effects on overall scapular morphology. Differences between shape and form spaces therefore underscore the contribution of size to developmental integration among scapular regions.

Along PC1, the youngest individuals displayed a scapula that was wider mediolaterally than tall superoinferiorly, with a relatively short SS and a narrow, elongated inferior two-thirds of the glenoid cavity. These features gradually transformed with increasing age, culminating in the oldest group, which exhibited a scapula that was taller superoinferiorly than wide mediolaterally, a SS that increased in length toward its lateral end and projected more prominently from the scapular body, and a glenoid cavity's inferior two-thirds wider mediolaterally than long superoinferiorly. Despite this sequential trend along PC1, substantial overlap between groups was observed in all analyses (Figures 4–6), underscoring the gradual and continuous nature of ontogenetic changes.

On PC2, in the ESM analysis, the most negative values corresponded to a relatively short supraspinous region in the superoinferior dimension, relative to the overall size of the scapular body, whereas the most positive values reflected a proportionally larger supraspinous area. In the SS analysis, positive PC2 values represented a SS that was wider superoinferiorly, shorter mediolaterally, and less curved at its upper lateral extremity. In the SGF analysis, PC2 described a transition from a narrower, elongated glenoid cavity (positive values) to a wider configuration (negative values). Taken together, these patterns indicate an ontogenetic trend characterized by the relative superoinferior elongation of the supraspinous fossa and the SS, accompanied by a progressive mediolateral widening of the SGF. Therefore, both PC1 and PC2 describe shape changes occurring throughout development. However, while PC1 captures the more general patterns of ontogenetic transformation, PC2 reflects more localized or specific aspects of morphological variation. Yet only PC1 consistently exhibited a sequential arrangement of the maturity groups. In this axis, during early infancy (maturity group 1), the scapula is relatively wide mediolaterally with a short spine, and the superior angle was inclined anteriorly. The inferior two-thirds of the SGF were narrow, elongated, and oriented caudally, with convex margins and a relatively flat surface (Figure 7).

Along PC1, all three analyses (ESM, SS, and SGF) revealed a consistent ontogenetic trajectory characterized by progressive changes in scapular proportions. Regarding the mean PC1 values corresponding to the first maturity group, observed in the ESM analysis, the scapula is relatively wide mediolaterally with a short spine, and the superior angle is inclined anteriorly. The inferior two-thirds of the glenoid cavity are narrow, elongated, and oriented caudally, with convex margins and a relatively flat surface (Figure 7). In the second maturity group, bipolar growth is established, marking the starting point for the SGF analysis (Figure 8). At this stage, the inferior portion of the glenoid cavity remains elongated but begins to widen anteriorly. In addition, the ESM analysis shows an increase in the distance between the superior margin of the inferior two-thirds of the glenoid cavity and the most medial point of the coracoid interface.

In the third maturity group, the ESM analysis shows elongation of the axillary border and a medial shift of the superior and inferior angles. Both the supraspinous and infraspinous regions expand, with a greater increase in height in the supraspinous region. The inferior two-thirds of the glenoid project more laterally and widen anteriorly, while the medial coracoid metaphysis also increases in height. In the SS analysis, the SS continues to lengthen, although its curvature remains relatively unchanged until the next stage.

In the fourth maturity group, the ESM analysis shows continued elongation of the axillary border, with the infraspinous region extending more superoinferiorly than the supraspinous region. The inferior portion of the glenoid cavity begins to project cranially, reversing the earlier trend observed in the first maturity group. Meanwhile, the SGF analysis indicates that the subcoracoid region expands in both height and width, forming a prominent inferior ridge that separates the upper third from the lower two-thirds of the glenoid cavity. At this maturity stage, the SS analysis begins to show more noticeable variation in curvature, with the spine starting to curve slightly anteriorly.

From the fifth to sixth maturity groups, the ESM analysis shows overlap between stages, whereas the SS and SGF analyses differentiate them more clearly (Figures 5 and 6). Combined shape data indicate marked increases in scapular height and width, driven by development of the medial border (Figure 7). The superior angle stabilizes, and the lower infraspinous fossa exhibits subtle anterior curvature. The SS continues to elongate and widen throughout adolescence, with more pronounced anterior curvature during mid- to late adolescence, particularly in the lateral portion of the spine. In the SGF

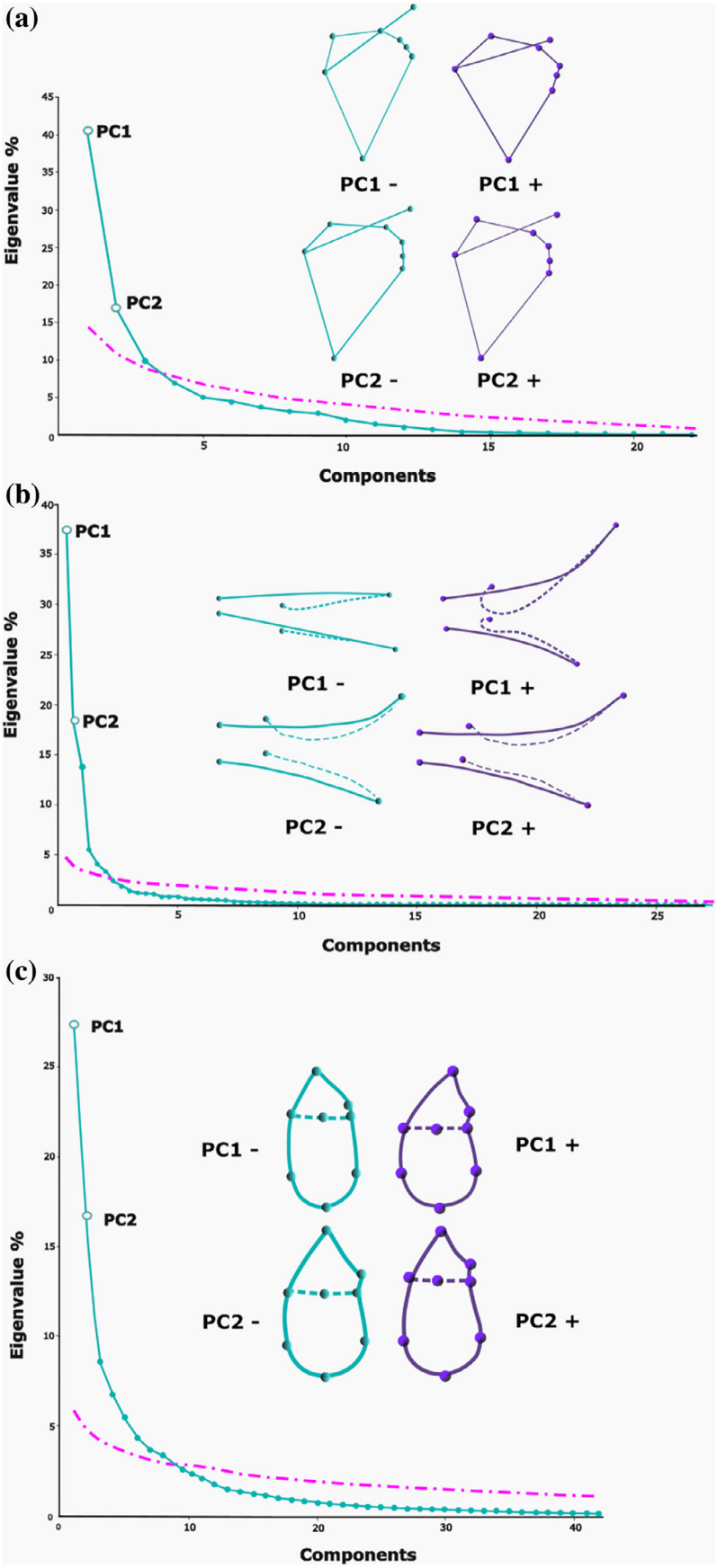

FIGURE 3 Principal component values. Broken stick values are indicated by a pink dashed line. (a) Analysis of the morphology of the complete scapula (entire scapular morphology). (b) Analysis of the morphology and curvature of the scapular spine. (c) Analysis of the morphology of the scapular glenoid fossa.

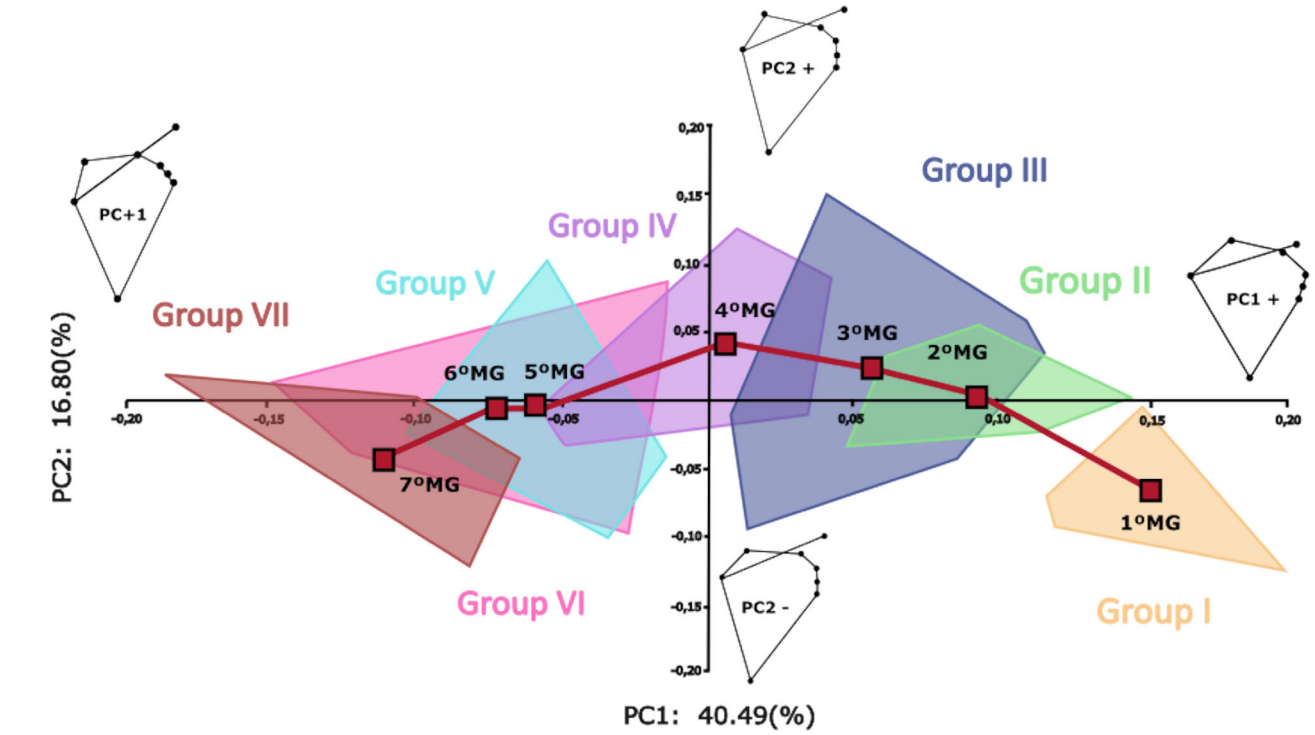

(a)

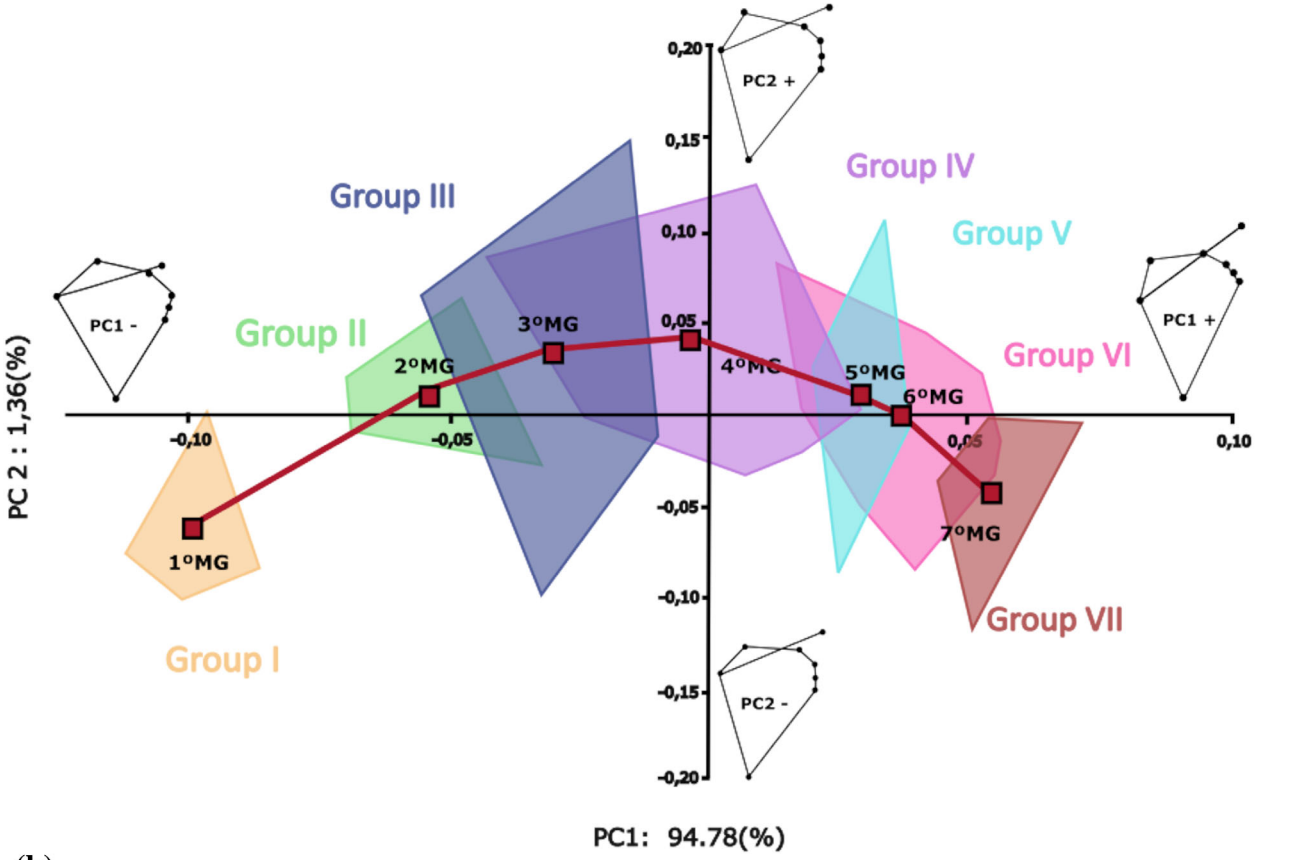

(b)

FIGURE 4 (a) Shape space analysis of the general scapular morphology, where the red line represents the mean center of each group. (b) Form space analysis of the general scapular morphology, with the red line indicating the mean center of each group.

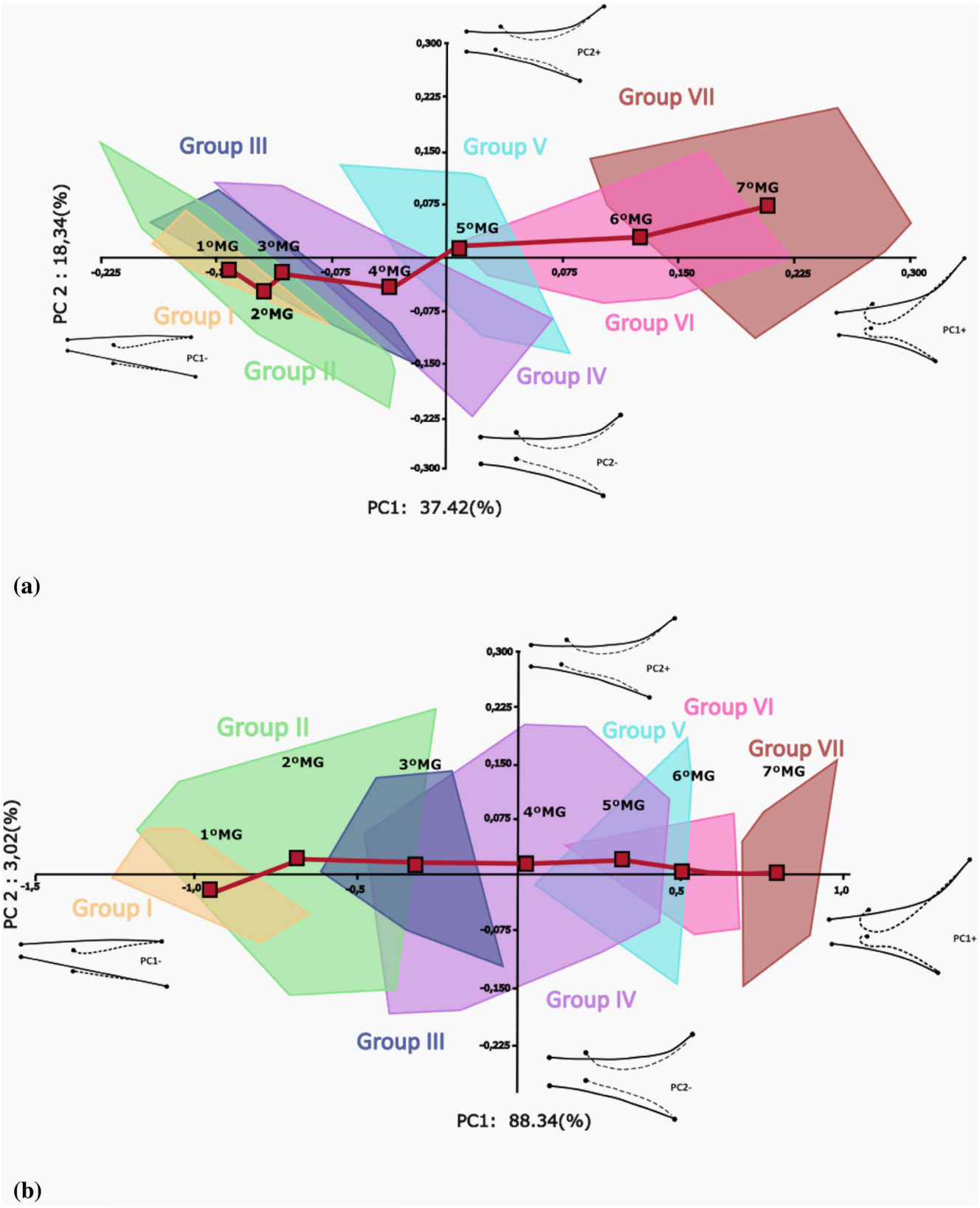

FIGURE 5 (a) Shape space analysis of the morphology and curvature of the scapular spine, where the red line represents the mean center of each group. (b) Form space analysis of the morphology and curvature of the scapular spine, with the red line indicating the mean center of each group.

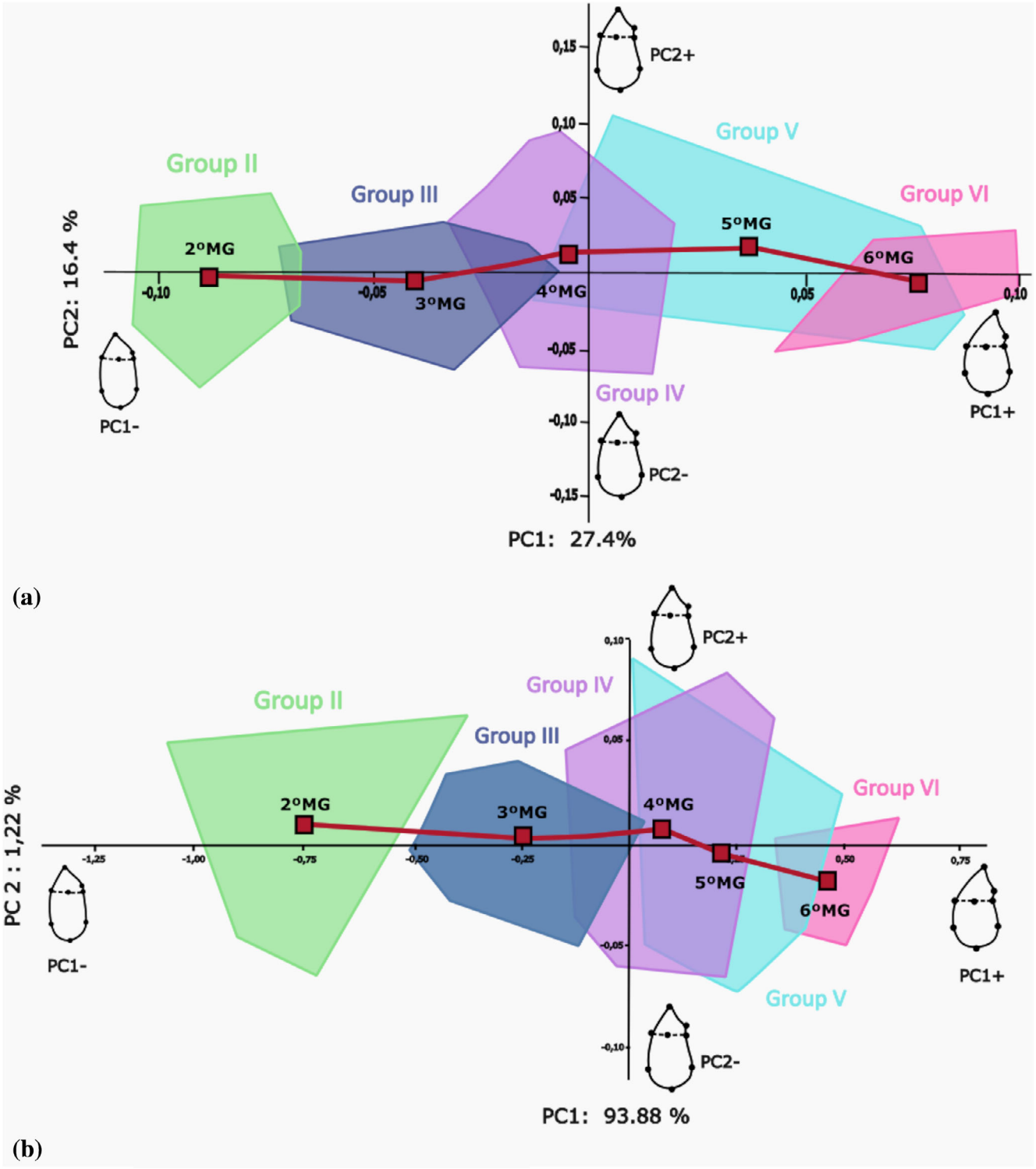

FIGURE 6 (a) Shape space analysis of subadult development of the glenoid cavity, where the red line represents the mean center of each group. (b) Form space analysis of subadult development of the glenoid cavity, with the red line indicating the mean center of each group.

analysis, during Group 5, the glenoid notch becomes increasingly elongated and curved, driven by lengthening of the coracoid interface and increased anterior curvature of both the subcoracoid and coracoid regions. The demarcation line between the upper third and lower two-thirds shifts laterally, while the inferior two-thirds of the glenoid cavity adopt a rounded morphology with balanced proportions, begin to develop a concave profile,

and shift cranially. Analysis of the sixth maturity group is limited to mid-adolescence, during which the inferior two-thirds of the glenoid cavity retain a rounded morphology with balanced proportions and continue developing a concave profile. Additionally, a marked anterior inclination becomes evident in both the coracoid interface and the adjacent portion of the subcoracoid region (Figure 8).

Transition to the mean values of the seventh maturity group is marked by elongation of the inferior angle. The SS continues to elongate, following a superior trajectory with increased anterior deviation (Figure 7). The inferior

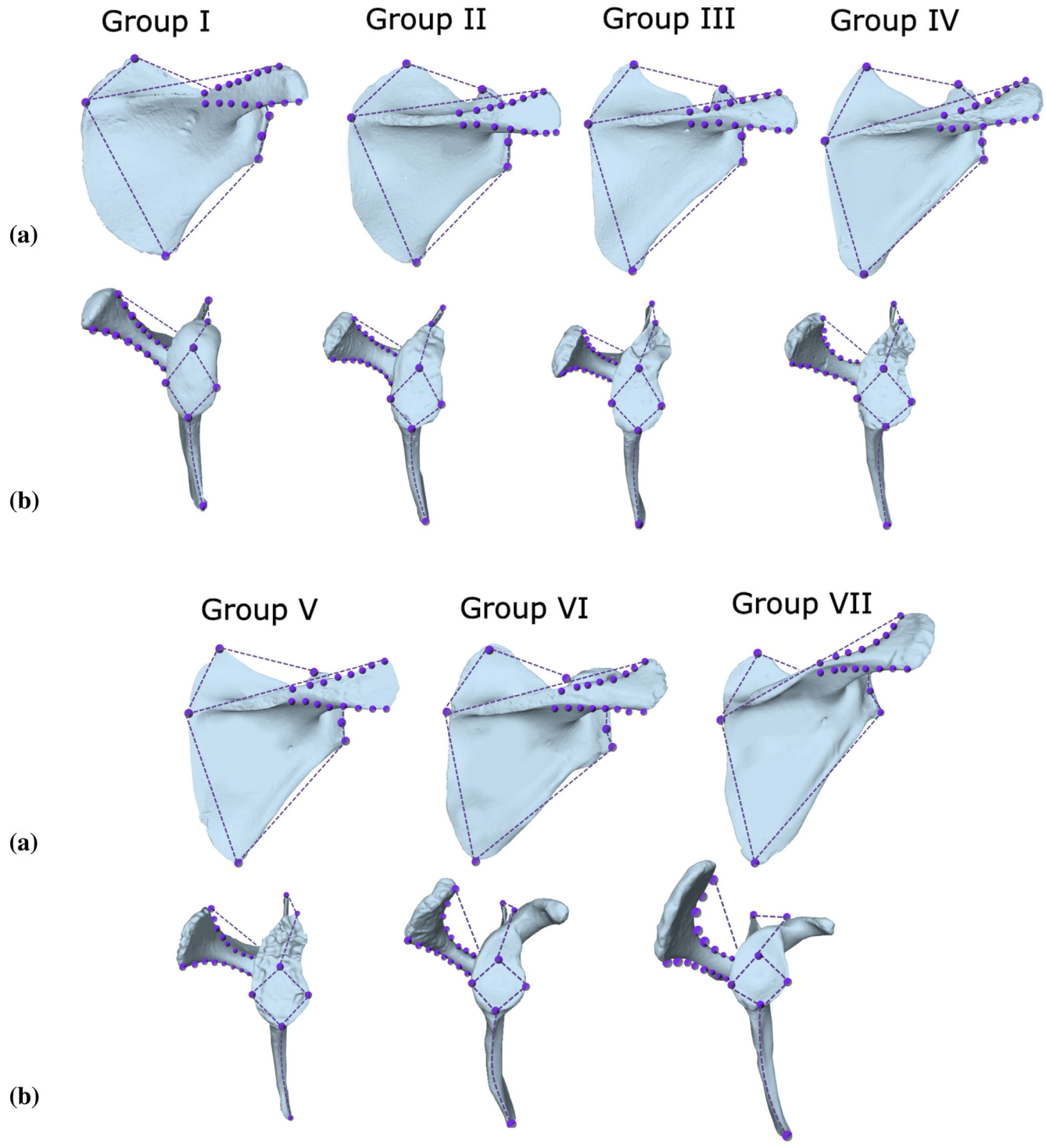

FIGURE 7 Legend on next page.

two-thirds of the glenoid cavity become wider than tall, with a cranially oriented and fully concave morphology (Figure 7).

4 | DISCUSSION

The present study set out to investigate ontogenetic changes in human scapular morphology by combining whole-bone and region-specific analyses. In particular, we aimed to evaluate how shape changes modulate scapular development across different ontogenetic stages, considering both the scapula as a whole and two of its most functionally relevant and archeologically recoverable regions: the SS and the SGF. Results indicate that, despite morphological overlaps between groups, especially in shape space, PC1 consistently revealed a temporal sequence of ontogenetic changes. In the youngest groups, the scapula was wider mediolaterally than tall superoinferiorly, with a short, thin, and straight SS and a narrow and elongated inferior two-thirds of the glenoid cavity. With increasing age, these traits gradually changed: the scapula became taller superoinferiorly than wide mediolaterally, the SS elongated toward its lateral end while shifting anteriorly and superiorly, and the inferior portion of the glenoid cavity widened mediolaterally. The same patterns of morphological change are also evident in the form space. However, because this space incorporates the effect of size, the proportion of variance explained is substantially higher, reflecting the combined influence of shape and growth-related variation. In some cases, this also results in a clearer differentiation among maturity groups. This is particularly evident for the first maturity group in the ESM analysis, which forms the most distinct cluster in the form space, mainly due to the rapid increase in overall size characteristic of early infancy (Figure 4). This pattern is consistent with previous findings based on linear measurements (Cardoso et al., 2017) and supports the view that the first year of life is characterized by accelerated growth that strongly influences overall scapular morphology.

In addition to these changes largely associated with overall growth, other aspects of scapular shape variation are likely influenced by biomechanical and functional factors, reflecting the progressive adaptation of the shoulder girdle to increasing mechanical demands during development. During early infancy (maturity group 1), the observed scapular morphology is consistent with a still-forming musculoskeletal framework, with limited mechanical input from the cervical spine and upper limb muscles. At this stage, the scapula is primarily shaped by intrinsic ossification patterns, with little influence from external biomechanical stimuli (Da Silva et al., 2016). For instance, the *levator scapulae* muscle, which inserts along the medial border of the supraspinous region, exerts relatively little mechanical traction during this stage due to the underdevelopment of the cervical vertebrae whose height is commonly used as a skeletal maturity indicator (Baccetti et al., 2005; Hassel & Farman, 1995; Mahmood et al., 2016; San Román et al., 2002). As a result, the supraspinous region remains short and curved toward anterior, shaped by both intrinsic ossification patterns and minimal muscular influence. Regarding the inferior two-thirds of the glenoid cavity, although the ossified surface appears relatively flat or even convex, the surrounding cartilage already exhibits a concave shape, anticipating the definitive articular morphology (Figure 8) (Gasbarro et al., 2017; Ogden & Phillips, 1983). This extensive cartilaginous scaffold not only prefigures future bone formation but also plays a crucial role in muscle attachment and joint stabilization (Carter & Wong, 2003; Grässel &

FIGURE 7 Morphological changes observed in the complete scapula and in the curvature of the mediolateral portion of the scapular spine over time. The shape change graphics obtained were superimposed onto scapulae belonging to the representative age groups. The scapulae do not represent the actual sizes according to age but are scaled based on the distance between the landmarks positioned at the superior and inferior angles. Group 1 (early infancy): The scapula is relatively wide mediolaterally, with a short spine. The inferior two-thirds of the glenoid cavity are narrow, elongated, and oriented caudally. Group 2 (late infancy): Onset of bipolar growth. The inferior two-thirds of the glenoid cavity retain their superoinferior elongation but begin to widen anteriorly and flatten. Group 3 (childhood): The axillary border elongates, and the superior and inferior angles shift medially. The supraspinous and infraspinous regions expand, particularly in height. The inferior two-thirds of the glenoid cavity widen and project laterally. The height of the most medial aspect of the coracoid metaphysis increases. The scapular spine lengthens, although its curvature remains unchanged. Group 4 (juveniles): The lateral border widens. The infraspinous region elongates more in the superoinferior direction than the supraspinous region. The inferior portion of the glenoid cavity begins to project cranially. Group 5 (early adolescence): Scapular height and width increase markedly. The superior angle stabilizes, and the lower infraspinous fossa exhibits a subtle anterior curvature. The spine elongates laterally and superiorly, beginning to exhibit anterior curvature. Group 6 (mid-late adolescence): Continued elongation of the spine, with pronounced anterior torsion. The inferior portion of the glenoid cavity shifts further cranially. Group 7 (adulthood): The inferior angle elongates inferiorly. The inferior two-thirds of the glenoid cavity become wider than tall, with a cranially oriented and fully concave morphology. The spine continues to elongate, extending upward and anteriorly. (a) Posterior view. (b) Lateral view.

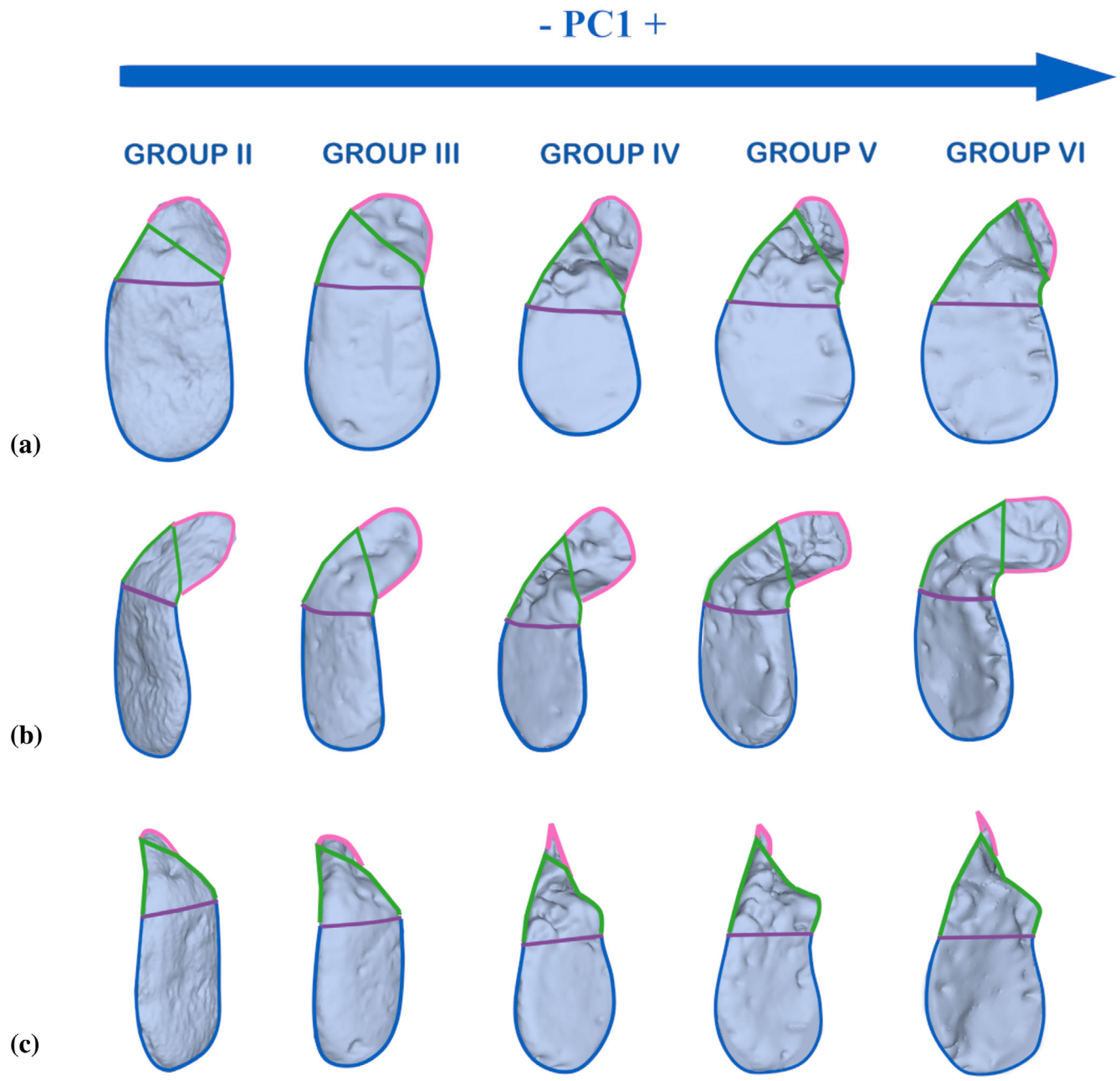

FIGURE 8 Sequence of shape changes in the subadult glenoid fossa along PC1 in lateral view (a), anterolateral view (b), and posterolateral view (c). A solid line outlines the overall contour. The area highlighted in blue corresponds to the inferior two-thirds of the glenoid cavity. The green outline delineates the subcoracoid region. The inner horizontal line, shown in purple, separates the inferior two-thirds of the glenoid cavity from the subcoracoid portion. The pink outline highlights the metaphyseal interface of the coracoid process.

Aszodi, 2016; Huang et al., 2004; Percival & Richtsmeier, 2017; Simpson & Augat, 2015).

During late infancy (maturity group 2), the most notable changes occur in the SGF. The inferior two-thirds of the glenoid cavity begin to widen anteriorly and lose their convexity. It is during this period that the bipolar growth interface becomes established (Ogden & Phillips, 1983). This interface forms with the development of the postnatally emerging primary ossification center of the scapula, the coracoid process, which typically appears before 1 year of age and gradually attains its characteristic hook-like shape, becoming morphologically recognizable around 3 years (Kothary et al., 2014; Scheuer & Black, 2004). Its growth induces a subtle anterior shift of the corresponding metaphyseal region within the bipolar growth plate and initiates a separation at the site where the first secondary ossification center of the scapula (the subcoracoid center) will later form. This developmental

event allows both interfaces to be analyzed separately, providing insights into scapular development through surfaces dependent on distinct ossification centers. Moreover, the coracoid process and the humeral head are the first ossification centers to appear in the shoulder (Figure 1), typically before the end of the first year (Kothary et al., 2014; Kwong et al., 2014; Ogden et al., 1978; Ogden & Phillips, 1983; Scheuer & Black, 2004), highlighting the structural and functional significance of this region from an early stage.

During the transition from infancy to childhood (maturity group 3), the scapula begins to elongate superoinferiorly (Figure 7). The changes observed coincide with increasing upright posture, greater upper limb use, and the onset of muscle activation (Scheuer & Black, 2004; Walicka-Cupryś et al., 2017). As the child develops greater motor control and coordination, the scapula undergoes geometric remodeling to accommodate increasing mechanical demands from muscles such as the *trapezius*, *serratus anterior*, and rhomboid muscles. The attachment areas of these muscles expand, and the surrounding bone surface remodels to withstand higher forces and changing directions of tension. At the same time, the progressive increase in shoulder mobility and adjustments in thoracic posture further contribute to shaping the overall scapular geometry during growth. (Dayanidhi et al., 2005; Jurimae & Jurimae, 2001; Struyf et al., 2010). Similar to other regions undergoing continuous development, such as the inferior angle, the chondro-osseous interface at the lateral end of the SS exhibits vascular-driven undulations that progressively increase its length, even before the appearance of any secondary ossification centers. These undulations reflect intrinsic bone development, gradually shaping the bone according to the pre-existing cartilaginous template and preparing it for subsequent epiphyseal fusion to form a complete structure (Ogden & Phillips, 1983).

During the juvenile period (maturity group 4), these trends continue with further vertical elongation of the scapular body (Figure 7). The infraspinous region expands more substantially than the supraspinous region, reflecting asymmetric muscular loading from increased activity of the *subscapularis* and *infraspinatus* muscles. The subcoracoid region becomes more prominent, and a distinct bulge forms along the inferior glenoid margin. The SS becomes more curved and begins its anterior torsion, likely reflecting enhanced mechanical loading from the deltoid and trapezius. In the upper region of the glenoid cavity, the subcoracoid metaphyseal surface undergoes both lateral and vertical expansion, beginning to replicate the developmental pattern of the overlying growth cartilage. This area develops vascular furrows indicative of active ossification. As these furrows extend, a distinct bulged demarcation line gradually forms, separating the upper third from the inferior two-thirds of the glenoid cavity (García-González, Rodríguez, Muñoz-Guarinos, et al., 2024; Scheuer & Black, 2004). Toward the end of the juvenility, we observe the emergence of the subcoracoid ossification center (Figure 1). This event, which in previous studies has been reported to occur between 8 and 10 years of age (Kothary et al., 2014; Scheuer & Black, 2004), is characterized by the appearance of small ossification foci that progressively coalesce into larger centers before ultimately fusing with the metaphysis (Ogden & Phillips, 1983). It has been demonstrated that metaphyseal regions undergo shape transformations in response to epiphyseal development (García-González et al., 2019; García-González, Rodríguez, Muñoz-Guarinos, et al., 2024; Knapik et al., 2022; Salazar-Fernández, Carretero, Quintino, et al., 2025; Walzer et al., 2014). This dynamic has been used to define maturity stages relevant for skeletal age estimation (Salazar-Fernández, Carretero, Quintino, et al., 2025), particularly in the context of the coracoid metaphysis at the glenoid–coracoid interface and its relationship to the epiphysis of the coracoid process (Salazar-Fernández, Carretero, Rodríguez, & García-González, 2025). Given the anatomical proximity of these elements to the subcoracoid region, the increase in developmental activity that we document here may represent a reliable morphological indicator of advancing skeletal maturity as it has been previously proposed by García-González, Rodríguez, Muñoz-Guarinos, et al. (2024).

By early adolescence (maturity group 5), the superior angle reaches its most medial position (Figure 7). The prominent demarcation line separating the upper third from the lower two-thirds of the SGF becomes increasingly projected laterally, while the inferior portion adopts more balanced proportions between height and width (Figures 7 and 8). The subcoracoid metaphyseal interface elongates laterally, and its posterior border increases in height, consistent with the gradual vertical growth of vascular undulations in this region (García-González, Rodríguez, Muñoz-Guarinos, et al., 2024). Similarly, the coracoid interface extends laterally, displaying a marked anterior inclination. Consequently, the anteromedial portion of the subcoracoid also inclines anteriorly (Figure 8). This anterior inclination has been described by Salazar-Fernández, Carretero, Rodríguez, and García-González (2025) as a gradual process beginning after preadolescence and becoming more pronounced in the final stage prior to fusion (Figure 1). The functional purpose is to position the coracoid in its anatomically mature orientation, allowing for the appropriate insertion and tensioning of the muscles and ligaments that begin to develop more prominently during adolescence (Salazar-

Fernández, Carretero, Rodríguez, & García-González, 2025). Altogether, these coordinated morphological changes contribute to the increased curvature and elongation of the glenoid notch, located along the anterior margin between the inferior two-thirds of the glenoid cavity and the subcoracoid region (Figures 7 and 8).

During the mid-late adolescence (maturity group 6), the inferior angle and lower infraspinous region of the scapula curve anteriorly, enhancing the convexity of the posterior aspect (Figure 7). The observed morphological transformation of the infraspinous region may reflect the increasing volume and functional demands of the *subscapularis* muscle (Bain et al., 2019; McCausland et al., 2022; Nordin & Frankel, 2001). From adolescence onward, the growing mass and activity of this muscle contribute to enhanced scapular stabilization as a component of the rotator cuff, enabling greater precision in rotational and elevation movements. This shift aligns with the broader developmental transition from the preadolescent phase, when scapulothoracic and glenohumeral joints are more flexible, to adulthood, where joint stability becomes essential for controlled and accurate upper limb motion (Dayanidhi et al., 2005). The SS undergoes its most pronounced curvature changes beginning in early adolescence and continuing through this developmental stage. Both the ESM and SS analyses capture these modifications, although they are less clearly expressed within the ESM framework. In ESM, changes are reflected primarily as an increase in spine length, observable when comparing the position of the most superolateral point of the lateral end of the SS with the medial reference point. Additionally, a deviation toward a more anterior and elevated plane becomes evident when contrasted with the position of the remaining scapular structures, positioning itself near the plane of the superior portion of the glenoid cavity.

By contrast, the curvature-specific analysis of the SS reveals more distinct and localized patterns (Figures 4 and 5). Specifically, while the inferior margin of the spine remains relatively straight, the superior margin progressively shifts anteriorly. The apparent superior expansion results from an increase in the superoinferior width of the lateral end of the spine. These morphological changes parallel the developmental dynamics of the acromion, which originates from distinct secondary ossification centers appearing between 14 and 16 years of age. These centers typically fuse to form three, and occasionally four, distinct components, which subsequently unite among themselves to form a structure that later fuses with the lateral end of the SS (Ogden & Phillips, 1983; Scheuer & Black, 2004). Complete fusion of the acromion generally occurs after 20 years, with the most active phase between 18 and 20 years (Ogden et al., 1979; Rockwood et al., 2016). Similar to the clavicle, although usually earlier, the acromion does not fully ossify until adulthood (Black & Scheuer, 1996; Scheuer & Black, 2004). However, significant morphological changes occur prior to adulthood, becoming most pronounced during adolescence, when they are closely linked to shoulder broadening and increased muscle mass, reflecting the strong interdependence between skeletal morphology and muscular function.

Development of the SGF during mid-late adolescence is generally complete by approximately 16 years of age, a period characterized by active ossification of the subcoracoid and coracoid processes (Ogden & Phillips, 1983). Between ages 14 and 16, the inferior two-thirds of the glenoid cavity gradually acquire a more rounded and concave morphology, alongside the elongation of the subcoracoid interface and increased definition of the glenoid notch. During this period, small ossification islands begin to appear along the rim of the inferior glenoid cavity, contributing to the formation of a more mature articular surface prior to complete epiphyseal fusion, which typically occurs between 17 and 18 years of age (Kothary et al., 2014; Scheuer & Black, 2004). The epiphyses of the subcoracoid and coracoid processes, together with that of the proximal humerus, tend to fuse around this age, marking a key milestone in the skeletal maturation of the glenohumeral joint. This fusion enhances the structural integration of the rotator cuff and strengthens the muscular insertions responsible for joint stabilization, particularly those of the *biceps brachii*. The short head of the *biceps brachii* muscle originates from the apex of the coracoid process, while the long head of the *biceps brachii* muscle arises from the supraglenoid tubercle in the superior third of the glenoid cavity (Nordin & Frankel, 2001).

Linear measurements of the glenoid by Rissech and Black (2007) indicate that the maximum length and width of the glenoid cavity, as well as the maximum length of the glenoid mass (including the glenoid–coracoid interface), are reliable age predictors up to 16 years. Additionally, Rissech and Black (2007) identify a phase of restricted growth previous to the adolescent acceleration of the glenoid cavity, estimated in their study to occur around 14–15 years of age. In our form space analysis (Figure 6), minimal size changes are observed between the fourth and fifth maturity groups, aligning with the proposed growth restriction phase before the glenoid cavity's rapid expansion at 14–15 years. This period of adolescent acceleration of the glenoid cavity, proposed by Rissech and Black (2007), coincides with the emergence of rim epiphyses in the glenoid cavity, likely contributing to an increase in its overall proportions, which also aligns with our results (Figures 7 and 8).

By early adulthood (maturity group 7), most shape transformations are complete. The SS reaches its final curvature and projection, the glenoid cavity adopts its mature concave form, and secondary ossification centers in the acromion and inferior angle fuse (Eovaldi & Varacallo, 2018; Gillen et al., 2019; Rauch et al., 2004). The final configuration of the scapula reflects the functional demands of adult musculoskeletal integration, supporting mature upper limb biomechanics, including load-bearing and precision movement. The rhomboid muscles connect the medial border of the scapula to the cervical and thoracic spine. The skeletal maturation of the medial border occurs in close temporal correspondence with that of the cervical vertebrae (with the exception of the axis), which typically completes their formation by early adulthood (Hassel & Farman, 1995; Morlesín, 2017; Rao et al., 2013; Roman,). Once the medial border and inferior angle are fully developed, the muscles attached to these regions benefit from stable bony insertions, improving both scapular support and mobility in late adolescence and early adulthood (Carter et al., 1996). These muscles are vital for retracting and rotating the scapula toward the vertebral column, thus enhancing scapular stability and upper limb movement (Nordin & Frankel, 2001). The secondary ossification center of the inferior angle appears toward the end of adolescence and begins fusing during early adulthood, in a manner similar to the ossification foci of the medial border (Ogden & Phillips, 1983; Scheuer & Black, 2004). Both events correlate with the heightened development of these areas during this final stage of skeletal maturation.

In sum, our results indicate that scapular development is not uniform but exhibits region-specific patterns of shape change. The SGF undergoes early modifications associated with articulation and mobility demands, whereas the SS shows later elongation and curvature changes related to muscle attachments and mechanical leverage. These findings suggest that modular growth in the scapula is driven by the interplay between intrinsic developmental programs and extrinsic functional demands, rather than occurring randomly or solely as a consequence of overall size increase.

5 | CONCLUSIONS

Analyses and findings in this study reinforce the value of using region-specific analyses to complement whole-bone assessments. Although the entire scapula provides a global view of growth dynamics, regional approaches capture morphological variation that may be obscured in full-bone analyses. This is particularly evident in both the SS, where curvature and torsion were only apparent in the localized shape analysis, and in the SGF, where the glenoid notch and subcoracoid region revealed detailed changes relevant to joint development.

In line with our initial hypothesis, our results confirm that scapular modularity during development arises from a combination of intrinsic and extrinsic factors. The scapula does not develop as a homogeneous structure depending solely on overall growth; instead, each module follows its own temporal and developmental trajectory. These timings are influenced not only by the appearance and fusion of ossification centers but also by pre-patterned developmental programs that guide the acquisition of adult functional morphology, preparing each region for final epiphyseal fusion. Morphological changes across regions also respond to biomechanical demands imposed by the joints to which they belong, as well as by neighboring structures through ligamentous and muscular attachments. Some regions are more responsive to musculoskeletal maturation, whereas others remain constrained by joint function. Regions with late-fusing secondary centers—such as the SS, inferior angle, and acromion—underwent more pronounced morphological transformations consistent with prolonged plasticity. By contrast, the SGF exhibited a more temporally restricted and morphologically stable developmental trajectory. Overall, the scapula transitions from a relatively unspecialized morphology to a configuration optimized for shoulder mobility and muscle attachment, characterized by an anteriorly and superiorly twisted SS, a more concave blade, a straighter and stronger superior angle, an anteriorly displaced coracoid, and a more rounded and concave glenoid fossa.

Additionally, the dual approach used in this study—combining whole-bone and region-specific analyses—highlights the value of a multi-scalar framework for understanding postnatal skeletal development. This perspective not only reveals how the scapula grows and adapts in vivo, but also enhances the interpretive potential of skeletal remains in forensic and bioarcheological contexts. When only isolated or fragmentary elements—such as the glenoid or SS—are preserved, region-specific analyses provide reliable developmental signals and offer practical alternatives for estimating age and assessing functional adaptation. The use of 3DGM was particularly effective in capturing both global and localized morphological changes across ontogeny, revealing differences that would otherwise remain undetected.

Future research should explore how factors such as sex, habitual activity, and pathological conditions influence scapular modularity, and extend comparative frameworks to extinct human species (fossil hominins) as well as non-human primates, in order to better understand evolutionary patterns of shoulder

development. Continued integration of 3DGM, muscle–bone interaction, and ossification timing will further refine our understanding of scapular growth and its variation across individuals, populations, and species.

AUTHOR CONTRIBUTIONS

Azahara Salazar-Fernández: Investigation; writing – original draft; methodology; validation; visualization; writing – review and editing; formal analysis; software; data curation. **José Miguel Carretero:** Writing – original draft; funding acquisition; validation; writing – review and editing; visualization; project administration; supervision; resources. **Laura Rodríguez:** Investigation; writing – original draft; visualization; writing – review and editing; methodology; supervision; formal analysis. **Rebeca García-González:** Conceptualization; investigation; writing – original draft; methodology; validation; visualization; writing – review and editing; formal analysis; data curation; supervision; resources; funding acquisition; software; project administration.

ACKNOWLEDGMENTS

We have benefitted from fruitful discussions with our colleagues from the Laboratorio de Evolución Humana at the University of Burgos. We are grateful to the Museo Aqueológico de Burgos (Junta de Castilla y León) for providing the study collections at our expense at the Laboratorio de Evolución Humana (LEH). We thank the Natural History Museum of Lisbon for granting access to the skeletal remains, which enabled the scanning and 3D modeling of the scapulae used in this study. We are also grateful to Maria Judite Silva Cardoso Alves for her assistance during data collection.

FUNDING INFORMATION

"Bioarqueología de la reproducción humana: una perspectiva evolutiva sobre los problemas actuales (JCYL BU010P24)" financed by Junta de Castilla y León and Fondo Europeo de Desarrollo Regional. The Atapuerca research project is financed by the Ministerio de Ciencia, Innovación y Universidades Grant PID2021-122355NB-C31 funded by MCIN/AEI/10.13039/501100011033 and "ERDF A way of making Europe."

ORCID

José Miguel Carretero https://orcid.org/0000-0003-0409-8087
Laura Rodríguez https://orcid.org/0000-0002-5090-1582
Rebeca García-González https://orcid.org/0000-0002-1035-6655

REFERENCES

Almécija, S., Pugh, K. D., Anaya, A., Smith, C. M., Simmons, N. B., Voss, R. S., Duncan, N., Lunde, D. P., Viera, M. K., Hsu, T., Gilissen, E., Maiolino, S. A., Winchester, J. M., Patel, B. A., Orr, C. M., Tocheri, M. W., Delson, E., Hammond, A. S., Boyer, D. M., & Catalano, S. A. (2024). Primate phenotypes: A multi-institution collection of 3D morphological data housed in MorphoSource. *Scientific Data*, *11*, 1391. https://doi.org/10.1038/s41597-024-04261-5

Baccetti, T., Franchi, L., & McNamara, J. A. (2005). The cervical vertebral maturation (CVM) method for the assessment of optimal treatment timing in dentofacial orthopedics. *Seminars in Orthodontics*, *11*, 119–129.

Bain, G. I., Phadnis, J., Itoi, E., Di Giacomo, G., Sugaya, H., Sonnabend, D. H., & McLean, J. (2019). Shoulder crane: A concept of suspension, stability, control and motion. *Journal of ISAKOS Joint Disorders & Orthopaedic Sports Medicine*, *4*(2), 63–70. https://doi.org/10.1136/jisakos-2017-000187

Bastir, M., García-Martínez, D., Recheis, W., Barash, A., Coquerelle, M., Rios, L., Peña-Melián, Á., García Río, F., & O'Higgins, P. (2013). Differential growth and development of the upper and lower human thorax. *PLoS One*, *8*(9), e75128. https://doi.org/10.1371/journal.pone.0075128

Black, S., & Scheuer, L. (1996). Age changes in the clavicle: From the early neonatal period to skeletal maturity. *International Journal of Osteoarchaeology*, *6*(5), 425–434. https://doi.org/10.1002/(SICI)1099-1212(199612)6:5<425::AID-OA287>3.0.CO;2-P

Bleuze, M. M., Wheeler, S. M., Williams, L. J., & Dupras, T. L. (2016). Growth of the pectoral girdle in a sample of juveniles from the kellis 2 cemetery, Dakhleh oasis, Egypt. *American Journal of Human Biology*, *28*(5), 636–645. https://doi.org/10.1002/ajhb.22844

Bogin, B. (2021). *Patterns of human growth* (Vol. 88, 3rd ed.). Cambridge University Press. https://doi.org/10.1017/9781108379977

Bookstein, F. L. (2018). *A course in morphometrics for biologists: Geometry and statistics for studies of organismal form*. https://www.amazon.com/Course-Morphometrics-Biologists-Statistics-Organismal/dp/1107190940

Cardoso, H. F. (2007). Environmental effects on skeletal versus dental development: Using a documented subadult skeletal sample to test a basic assumption in human osteological research. *American Journal of Physical Anthropology*, *132*(2), 223–233. https://doi.org/10.1002/ajpa.20482

Cardoso, H. F. V. (2006). Brief communication: The collection of identified human skeletons housed at the Bocage Museum (National Museum of Natural History), Lisbon, Portugal. *American Journal of Physical Anthropology*, *129*(2), 173–176. https://doi.org/10.1002/ajpa.20228

Cardoso, H. F. V., Abrantes, J., & Humphrey, L. T. (2014). Age estimation of immature human skeletal remains from the diaphyseal length of the long bones in the postnatal period. *International Journal of Legal Medicine*, *128*(5), 809–824. https://doi.org/10.1007/s00414-013-0925-5

Cardoso, H. F. V., Spake, L., & Humphrey, L. T. (2017). Age estimation of immature human skeletal remains from the dimensions of the girdle bones in the postnatal period. *American Journal of Physical Anthropology*, *163*(4), 772–783. https://doi.org/10.1002/ajpa.23248

Carter, D. R., & Wong, M. (2003). Modelling cartilage mechanobiology. *Philosophical Transactions of the Royal Society B: Biological*

Sciences, *358*(1437), 1461–1471. https://doi.org/10.1098/rstb.2003.1346

Carter, D. R., Van Der Meulen, M. C. H., & Beaupré, G. S. (1996). Mechanical factors in bone growth and development. *Bone*, *18*(1 Suppl), S5–S10. https://doi.org/10.1016/8756-3282(95)00373-8

Churchill, S. E., & Rhodes, J. A. (2009). The evolution of the human capacity for "killing at a distance": The human fossil evidence for the evolution of projectile weaponry. In *Vertebrate paleobiology and paleoanthropology series* (pp. 201–210). Springer. https://doi.org/10.1007/978-1-4020-9699-0_15

Churchill, S. E., & Trinkaus, E. (1990). Neandertal scapular glenoid morphology. *American Journal of Physical Anthropology*, *83*(2), 147–160. https://doi.org/10.1002/ajpa.1330830203

Conceição, E., & Cardoso, H. (2011). Environmental effects on skeletal versus dental development II: Further testing of a basic assumption in human osteological research. *American Journal of Physical Anthropology*, *144*(3), 463–470. https://doi.org/10.1002/ajpa.21433

Cowgill, L. W., Warrener, A., Pontzer, H., & Ocobock, C. (2010). Waddling and toddling: The biomechanical effects of an immature gait. *American Journal of Physical Anthropology*, *143*(1), 52–61. https://doi.org/10.1002/ajpa.21289

Da Silva, E. S. M., Santos, G. L. D., Greco, A. L. R., & Tudella, E. (2016). Influence of different sitting positions on healthy infants' reaching movements. *Journal of Motor Behavior*, *49*(6), 603–610. https://doi.org/10.1080/00222895.2016.1247034

Dayanidhi, S., Orlin, M., Kozin, S., Duff, S., & Karduna, A. (2005). Scapular kinematics during humeral elevation in adults and children. *Clinical Biomechanics*, *20*(6), 600–606. https://doi.org/10.1016/j.clinbiomech.2005.03.002

Demirjian, A., Goldstein, H., & Tanner, J. M. (1973). A new system of dental age assessment. *Human Biology*, *45*(2), 211–227.

Di Vincenzo, F., Churchill, S. E., & Manzi, G. (2012). The Vindija Neanderthal scapular glenoid fossa: Comparative shape analysis suggests evo-devo changes among neanderthals. *Journal of Human Evolution*, *62*(2), 274–285. https://doi.org/10.1016/j.jhevol.2011.11.010

Eovaldi, B. J., & Varacallo, M. (2018). *Anatomy, shoulder and upper limb, shoulder muscles*. StatPearls.

Freidline, S. E., Gunz, P., Harvati, K., & Hublin, J. (2013). Evaluating developmental shape changes in *Homo antecessor* subadult facial morphology. *Journal of Human Evolution*, *65*(4), 404–423. https://doi.org/10.1016/j.jhevol.2013.07.012

Frelat, M. A., Coquerelle, M., & Trinkaus, E. (2017). Ontogeny of modern human longitudinal body and transverse shoulder proportions. *American Journal of Human Biology*, *29*(2), e22925. https://doi.org/10.1002/ajhb.22925

Frontier, S. (1976). Étude de la décroissance des valeurs propres dans une analyse en composantes principales: Comparaison avec le modèle du bâton brisé. *Journal of Experimental Marine Biology and Ecology*, *25*(1), 67–75.

García-González, R. (2013). *Estudio Comparativo de los Patrones de Crecimiento y Desarrollo Corporal en Humanos Actuales y Fósiles a Partir Del Análisis de Los Huesos Largos*. [Unpublished PhD dissertation]. Burgos University.

García-González, R., Carretero, J. M., Rodríguez, L., & Arsuaga, J. L. (2019). Two new methodological approaches for assessing skeletal maturity in archeological human remains based on the femoral distal epiphysis. *Archaeological and Anthropological Sciences*, *11*(12), 6515–6536. https://doi.org/10.1007/s12520-019-00920-6

García-González, R., Carretero, J. M., Rodríguez, L., Gómez-Olivencia, A., Arsuaga, J. L., de Castro, J. M. B., Carbonell, E., Martínez, I., & Lorenzo, C. (2009). Étude Analytique D'une Clavicule Complète de Subadulte D'homo Antecessor (Site de Gran Dolina, Sierra d'Atapuerca, Burgos, Espagne). *L' Anthropologie*, *113*(1), 222–232. https://doi.org/10.1016/j.anthro.2008.12.002

García-González, R., Rodríguez, L., Muñoz-Guarinos, J., Sánchez-Puente, Z., Fernández-Viejo, M., Cirotto, N., Navarro-Pérez, A., García Barreiro, M., Salazar-Fernández, A., Quintino, Y., Adán Álvarez, G., & Carretero, J. M. (2024). *Paleodemographic profiles of the populations buried in San Pablo convent (Burgos, Spain)*. ENTEMU, XX.

García-González, R., Rodríguez, L., Salazar-Fernández, A., Arsuaga, J. L., & Carretero, J. (2024). Updated study of adult and subadult pectoral girdle bones from Sima de los Huesos site (Sierra de Atapuerca, Burgos, Spain): Anatomical and age estimation keys. *Anatomical Record*, *307*, 2491–2518. https://doi.org/10.1002/ar.25158

Gasbarro, G., Bondow, B., & Debski, R. (2017). Clinical anatomy and stabilizers of the glenohumeral joint. *Annals of Joint*, *2*, 58. https://doi.org/10.21037/aoj.2017.10.03

Gillen, Z. M., Shoemaker, M. E., McKay, B. D., Bohannon, N. A., Gibson, S. M., & Cramer, J. T. (2019). Muscle strength, size, and neuromuscular function before and during adolescence. *European Journal of Applied Physiology*, *119*(7), 1619–1632. https://doi.org/10.1007/s00421-019-04151-4

Grässel, S., & Aszodi, A. (Eds.). (2016). *Cartilage: Volume 1: Physiology and development* (1st ed.). Springer International Publishing. Google Scholar

Green, D. J., & Alemseged, Z. (2012). Australopithecus afarensis scapular ontogeny, function, and the role of climbing in human evolution. *Science*, *338*(6106), 514–517. https://doi.org/10.1126/science.1227123

Gunz, P., & Mitteroecker, P. (2013). Semilandmarks: A method for quantifying curves and surfaces. *Hystrix, the Italian Journal of Mammalogy*, *24*(1), 103–109. https://doi.org/10.4404/hystrix-24.1-6292

Gunz, P., Mitteroecker, P., & Bookstein, F. L. (2006). Semilandmarks in three dimensions. In *Modern morphometrics in physical anthropology* (pp. 73–98). Kluwer Academic Publishers. https://doi.org/10.1007/0-387-27614-9_3

Hammer-Muntz, O., Harper, D., & Ryan, P. (2001). *PAST: Paleontological statistics software package for education and data analysis (Version 2.09)*. Palaeontologia Electronica. http://scienceopen.com/document?vid=f7c81409-9131-4ded-a3d6-e1509342d3df

Hassel, B., & Farman, A. G. (1995). Skeletal maturation evaluation using cervical vertebrae. *American Journal of Orthodontics and Dentofacial Orthopedics*, *107*(1), 58–66. https://doi.org/10.1016/s0889-5406(95)70157-5

Huang, C., Stankiewicz, A., Ateshian, G. A., & Mow, V. C. (2004). Anisotropy, inhomogeneity, and tension–compression nonlinearity of human glenohumeral cartilage in finite deformation. *Journal of Biomechanics*, *38*(4), 799–809. https://doi.org/10.1016/j.jbiomech.2004.05.006

Humphrey, L. (2000). Growth studies of past populations: An overview and an example. In M. Cox & M. Mays (Eds.), *Human osteology in archaeology and forensic science* (pp. 23–38). Cambridge University Press.

Humphrey, L. T. (1998). Growth patterns in the modern human skeleton. *American Journal of Physical Anthropology*, *105*(1), 57–72.

Jurimae, T., & Jurimae, J. (2001). *Growth, physical activity, and motor development in prepubertal children*. CRC Press. https://doi.org/10.1201/b14219

Klingenberg, C. P. (2011). MorphoJ: An integrated software package for geometric morphometrics. *Molecular Ecology Resources*, *11*(2), 353–357. https://doi.org/10.1111/j.1755-0998.2010.02924.x

Knapik, D. M., Do, T. M., Fausett, C. L., & Liu, R. W. (2022). An anatomic and 3D study of the development of the proximal humeral physis. *Surgical and Radiologic Anatomy*, *44*(6), 869–876. https://doi.org/10.1007/s00276-022-02946-3

Kothary, S., Rosenberg, Z. S., Poncinelli, L. L., & Kwong, S. (2014). Skeletal development of the glenoid and glenohumeral interface in the pediatric population: MRI features. *Skeletal Radiology*, *43*(9), 1281–1288. https://doi.org/10.1007/s00256-014-1936-0

Kwong, S., Kothary, S., & Poncinelli, L. L. (2014). Skeletal development of the proximal humerus in the pediatric population: MRI features. *American Journal of Roentgenology*, *202*(2), 418–425. https://doi.org/10.2214/AJR.13.10711

Liversidge, H. M., & Molleson, T. (2004). Variation in crown and root formation and eruption of human deciduous teeth. *American Journal of Physical Anthropology*, *123*(2), 172–180. https://doi.org/10.1002/ajpa.10318

Liversidge, H. M., Chaillet, N., Mörnstad, H., Nyström, M., Rowlings, K., Taylor, J., & Willems, G. (2006). Timing of Demirjian's tooth formation stages. *Annals of Human Biology*, *33*(4), 454–470. https://doi.org/10.1080/03014460600802387

Liversidge, H. M., Smith, B. H., & Maber, M. (2010). Bias and accuracy of age estimation using developing teeth in 946 children. *American Journal of Physical Anthropology*, *143*(4), 545–554. https://doi.org/10.1002/ajpa.21349

López-Costas, O., Rissech, C., Trancho, G., & Turbón, D. (2012). Postnatal ontogenesis of the tibia. Implications for age and sex estimation. *Forensic Science International*, *214*(1–3), 207.e1–207.e11. https://doi.org/10.1016/j.forsciint.2011.07.038

Lozano-Bendicho, C., Sánchez-Andrés, Á., Martínez, I., Conde-Valverde, M., Carretero, J., Rodríguez, L., Cirotto, N., & García-González, R. (2025). Occipital bone modeling patterns during the first years of life: A preliminary histological and quantitative approach. *Journal of Anatomy*, *247*, 885–896. https://doi.org/10.1111/joa.14206

Mahmood, H. T., Shaikh, A., & Fida, M. (2016). Association between frontal sinus morphology and cervical vertebral maturation for the assessment of skeletal maturity. *American Journal of Orthodontics and Dentofacial Orthopedics*, *150*(4), 637–642. https://doi.org/10.1016/j.ajodo.2016.03.022

McCausland, C., Sawyer, E., Eovaldi, B. J., & Varacallo, M. (2022). Anatomy, shoulder and upper limb, shoulder muscles. In *StatPearls*. StatPearls Publishing.

McGraw, M. A., Mehlman, C. T., Lindsell, C. J., & Kirby, C. L. (2009). Postnatal growth of the clavicle: Birth to 18 years of age. *Journal of Pediatric Orthopaedics*, *29*(8), 937–943. https://doi.org/10.1097/BPO.0b013e3181c11992

Mitteroecker, P., & Gunz, P. (2009). Advances in geometric morphometrics. *Evolutionary Biology*, *36*(2), 235–247. https://doi.org/10.1007/s11692-009-9055-x

Mitteroecker, P., Gunz, P., Bernhard, M., Schaefer, K., & Bookstein, F. L. (2004). Comparison of cranial ontogenetic trajectories among great apes and humans. *Journal of Human Evolution*, *46*(6), 679–698. https://doi.org/10.1016/j.jhevol.2004.03.006

Mori, T., & Harvati, K. (2019). Basicranial ontogeny comparison in pan troglodytes and *Homo sapiens* and its use for developmental stage definition of KNM-ER 42700. *American Journal of Physical Anthropology*, *170*(4), 579–594. https://doi.org/10.1002/ajpa.23926

Morlesín, M. C. (2017). La maduración vertebral: método complementario para la estimación de la edad en restos óseos humanos. *La Zaranda de Ideas: Revista de Jóvenes Investigadores en Arqueología*, *15*(2), 95–112.

Muñoz-Guarinos, J., Rodríguez, L., Carretero, J. M., & García-González, R. (2025). Exploring developmental changes in femoral midneck cross-sectional properties. *The Anatomical Record*, *308*, 2212–2233. https://doi.org/10.1002/ar.25618

Nordin, M., & Frankel, V. (2001). *Basic biomechanics of the musculoskeletal system* (3rd ed.). Lippincott Williams & Wilkins.

Ogden, J. A., & Phillips, S. B. (1983). Radiology of postnatal skeletal development. VII. The scapula. *Skeletal Radiology*, *9*(3), 157–169.

Ogden, J. A., Conlogue, G. J., & Bronson, M. L. (1979). Radiology of postnatal skeletal development. III. The clavicle. *Skeletal Radiology*, *4*(4), 196–203. https://doi.org/10.1007/bf00347213

Ogden, J. A., Conlogue, G. J., & Jensen, P. (1978). Radiology of postnatal skeletal development: The proximal humerus. *Skeletal Radiology*, *2*(3), 153–160. https://doi.org/10.1007/BF00347314

Percival, C. J., & Richtsmeier, J. T. (2017). Building Bones: Bone Formation and Development in Anthropology. *En Cambridge University Press eBooks*. https://doi.org/10.1017/9781316388907

Rao, R. D., Tang, S., Lim, C., & Yoganandan, N. (2013). Developmental morphology and ossification patterns of the C1 vertebra. *Journal of Bone and Joint Surgery*, *95*(17), e124. https://doi.org/10.2106/jbjs.l.01035

Rauch, F., Bailey, D. A., Baxter-Jones, A., Mirwald, R., & Faulkner, R. (2004). The 'muscle-bone unit' during the pubertal growth spurt. *Bone*, *34*(5), 771–775. https://doi.org/10.1016/j.bone.2004.01.022

Rissech, C., & Black, S. (2007). Scapular development from the neonatal period to skeletal maturity: A preliminary study. *International Journal of Osteoarchaeology*, *17*(5), 451–464. https://doi.org/10.1002/oa.890

Rissech, C., López-Costas, O., & Turbón, D. (2013). Humeral development from neonatal period to skeletal maturity—Application in age and sex assessment. *International Journal of Legal Medicine*, *127*(1), 201–212. https://doi.org/10.1007/s00414-012-0713-7

Rissech, C., Schaefer, M., & Malgosa, A. (2008). Development of the femur—Implications for age and sex determination. *Forensic Science International*, *180*(1), 1–9. https://doi.org/10.1016/j.forsciint.2008.06.006

Roche, A. F. (1992). *Growth, maturation, and body composition: The Fels Longitudinal Study 1929–1991*. Cambridge University Press.

Rockwood, C. A., Matsen, F. A., Wirth, M. A., Lippitt, S. B., Fehringer, E. V., & Sperling, J. W. (2016). *Rockwood and Matsen's the shoulder*. Elsevier. https://doi.org/10.1016/B978-0-323-29731-8.00023-4

Rohlf, F. J., & Slice, D. (1990). Extensions of the Procrustes method for the optimal superimposition of landmarks. *Systematic Zoology*, *39*(1), 40–59. https://doi.org/10.2307/2992207

Rosas, A., Ríos, L., Estalrrich, A., Liversidge, H., García-Tabernero, A., Huguet, R., Cardoso, H., Bastir, M., Lalueza-Fox, C., de la Rasilla, M., & Dean, C. (2017). The growth pattern of neandertals, reconstructed from a juvenile skeleton from El Sidrón (Spain). *Science*, *357*(6357), 1282–1287. https://doi.org/10.1126/science.aan6463

Salazar-Fernández, A., Carretero, J. M., Quintino, Y., Harvati, K., Rodríguez, L., & García-González, R. (2025). Pre-fusion shape changes of humeral metaphyseal surfaces: A new method for assessing maturity and age in non-adult skeletal individuals. *American Journal of Physical Anthropology*, *186*(1), e25063. https://doi.org/10.1002/ajpa.25063

Salazar-Fernández, A., Carretero, J. M., Rodríguez, L., & García-González, R. (2025). Morphological development and maturity assessment of the coracoid process and its fusion site on the glenoid-coracoid interface. *Journal of Bioanthropology*, *4*(3), 6–23. https://doi.org/10.54062/jb.4.3.3

San Román, P., Palma, J. C., Oteo, M. D., & Nevado, E. (2002). Skeletal maturation determined by cervical vertebrae development. *European Journal of Orthodontics*, *24*(3), 303–311. https://doi.org/10.1093/ejo/24.3.303

Scheuer, L., & Black, S. (2000). Bone development. In *Developmental juvenile osteology*. Elsevier Academic Press.

Scheuer, L., & Black, S. (2004). *The juvenile skeleton*. Elsevier Science.

Simpson, H., & Augat, P. (2015). *Experimental research methods in orthopedics and trauma*. Georg Thieme Verlag. https://doi.org/10.1055/b-0035-122000

Slice, D. (2005). *Modern morphometrics in physical anthropology*. Springer New York. https://doi.org/10.1007/0-387-27614-9

Stratovan Corporation. (2018). *Stratovan Pro Surgical 3D* [Software]. Version 2018.08.07. https://www.stratovan.com/products/pro-surgical-3d

Struyf, F., Nijs, J., Horsten, S., Mottram, S., Truijen, S., & Meeusen, R. (2010). Scapular positioning and motor control in children and adults: A laboratory study using clinical measures. *Manual Therapy*, *16*(2), 155–160. https://doi.org/10.1016/j.math.2010.09.002

Stull, K. E., L'Abbé, E. N., & Ousley, S. D. (2014). Using multivariate adaptive regression splines to estimate subadult age from diaphyseal dimensions. *American Journal of Physical Anthropology*, *154*(3), 376–386. https://doi.org/10.1002/ajpa.22522

Trinkaus, E. (1977). A functional interpretation of the axillary border of the neandertal scapula. *Journal of Human Evolution*, *6*(3), 231–234. https://doi.org/10.1016/S0047-2484(77)80047-X

Walicka-Cupryś, K., Drzał-Grabiec, J., Rachwał, M., Piwoński, P., Perenc, L., Przygoda, Ł., & Zajkiewicz, K. (2017). Body posture asymmetry in prematurely born children at six years of age. *BioMed Research International*, *2017*, 9302520. https://doi.org/10.1155/2017/9302520

Walzer, S. M., Cetin, E., Grübl-Barabas, R., Sulzbacher, I., Rueger, B., Girsch, W., Toegel, S., Windhager, R., & Fischer, M. B. (2014). Vascularization of primary and secondary ossification centres in the human growth plate. *BMC Developmental Biology*, *14*, 36. https://doi.org/10.1186/s12861-014-0036-7

Young, N. (2004). Modularity and integration in the hominoid scapula. *Journal of Experimental Zoology Part B Molecular and Developmental Evolution*, *302B*(3), 226–240. https://doi.org/10.1002/jez.b.21003

Young, N. M. (2006). Function, ontogeny and canalization of shape variance in the primate scapula. *Journal of Anatomy*, *209*(5), 623–636. https://doi.org/10.1111/j.1469-7580.2006.00639.x

Young, N. M. (2008). A comparison of the ontogeny of shape variation in the anthropoid scapula: Functional and phylogenetic signal. *American Journal of Physical Anthropology*, *136*(3), 247–264. https://doi.org/10.1002/ajpa.20799

How to cite this article: Salazar-Fernández, A., Carretero, J. M., Rodríguez, L., & García-González, R. (2026). Integrating whole-bone and regional analyses to understand human scapular growth. *The Anatomical Record*, 1–23. https://doi.org/10.1002/ar.70156